1-1-1983

Thermoplastic damage of a stretched plate heated by a moving energy source.

Metin Ozen

THERMOPLASTIC DAMAGE OF A STRETCHED PLATE HEATED BY A MOVING ENERGY SOURCE

by

Metin Ozen

A Thesis

Presented to the Graduate Committee

of Lehigh University

in Candidacy for the Degree of

Master of Science

in

Applied Mechanics

Lehigh University

1983

This thesis is accepted and approved in partial fulfillment of the requirement for the degree of Master of Science.

Sept. 8, 1983
(date)

George C. Sih
Professor in Charge

Chairman of Department

ACKNOWLEDGEMENTS

The author wishes to express his gratitude to his advisor, Professor George C. Sih, for his support which made this work possible.

The support and encouragement of the Naval Research Laboratory is also acknowledged.

Professor Marek Matczyński's knowledge of thermoelasticity and his helpful advice are greatly appreciated.

Also, thanks to Mrs. Barbara DeLazaro for her patience and care in the preparation of this thesis.

TABLE OF CONTENTS

LIST OF TABLES

LIST OF FIGURES

LIST OF FIGURES - (CONTINUED)

LIST OF FIGURES - (CONTINUED)

ABSTRACT

Thermoplastic stress analysis is made for the problem of a moving energy source impinging on a stretched plate. The method of finite element is applied such that the motion of the heat source is discretized into a finite number of time increments. The energy source may represent a laser beam with a high local intensity such that the material deforms beyond its elastic limit and experiences permanent damage by evaporation. This reduces the local stiffness and may lead to global instability.

A failure analysis is also performed by application of the strain energy density theory which was incorporated with the incremental theory of thermoplasticity. The specific example involves a 7075-T651 aluminum plate subjected to tensile loading of 2.179×10^2 MPa. The energy source is assumed to have a radius of 1.65 cm and to travel at a velocity of 63.5 cm/sec along the line of symmetry being normal to the direction of applied tension. The possible failure location is predicted for each increment of time by analyzing the fluctuation of the local strain energy density field. A critical point corresponding to incipient fracture is found when the energy source traveled approximately two thirds of its way across the plate width which is 45.72 cm. The length is 55.88 cm. This result is consistent phenomenon observed experimentally by the Naval Research Laboratory.

CHAPTER I - INTRODUCTION

Lasers have found numerous applications in industry since their invention in 1960. Today, lasers are being used widely in the fields of welding, hole drilling and cutting. Their coherent light intensity can be focused along predetermined trajectory for welding and cutting. By controlling the energy intensity and field depth, lasers can also enhance the fatigue life of metals by evaporating a more uniform layer of material on the surface.

A laser is a device which produces a coherent beam of light at a specific wavelength [1]. Ordinary light sources scatter in all directions and usually possess a large range of wavelengths. Laser, however, is highly monochromatic and directional. It is highly collimated with high wavelength purity. With these properties, laser beam can be focused to an intense spot which can be used to enhance material properties or to create controlled damage in material.

The conversion of this intense energy to thermal work is governed by the transfer of heat from the source to the target [2]. A mathematical model is developed in this work to investigate its influence on material damage and structural integrity. The heat transfer portion of the problem may be resolved by employing the Galilean transformation such that the time dependence can be eliminated in the heat conduction equation. The advantage of this treatment is that the problem is reduced to a steady state case since the observer is to move with the heat source. Once the temperature distribution is

known, the thermal stresses can be found as shown by Sih and Matczyński [3]. However, the model of an instantaneous point source does not realistically simulate the effect of laser [4] whose beam diameter acquires a finite radius. The idealized model must therefore be modified by using the point source solution as a Green's function.

In addition to the intensity and velocity, the damaged zone behind a moving laser source depends on the beam diameter. The material ahead of the traveling energy source also undergoes local yielding and behaves nonlinearly. Therefore, damage is cumulative and load history dependent. In this respect, theory of elasticity will not hold. Many of the classical failure criteria such as maximum normal stress*, maximum normal strain, etc., also fail to apply because they lead to inconsistent predictions. Even though the final failure is due to crack propagation, crack initiation process occurs so rapidly that it is not impossible to identify a crack size. This leaves much doubt on the application of linear elastic fracture mechanics (LEFM). Besides, the K_{1c} or G_{1c} concept in LEFM is not valid in the presence of substantial plastic deformation.

It is therefore essential to select a rational and self-consistent failure criterion that can handle complex geometries, different materials (elastic or plastic), and general loading conditions. Sih's [5] Strain Energy Density (SED) Criterion is most suitable since it does

*For example, the direction of maximum local normal stress is parallel to a moving crack which contradicts the initial assumption of being perpendicular to the direction of crack propagation.

not rely on force-fitting experimental data and it has the capability of relating local and global failure modes. Moreover, Sih's theory does not require a precise location and size of an initial flaw which, on the other hand, is a necessity for the LEFM approach. Sih's theory accounts for yielding and fracture simultaneously by examining the stationary values of the strain energy density function dW/dV near a critical location. The critical strain energy density function $(dW/dV)_c$ is assumed to be a material constant and can be evaluated from the area under the true stress and strain curve. It can be used to predict the fracture initiation of an elastic element near the critical location. When the element yields before fracture, $(dW/dV)_c$ must be modified to $(dW/dV)_c^*$ as the plastic energy density is no longer available for release at fracture.

In this work, SED criterion is applied to predict the failure location of the material in front of the laser beam. Damage of the material behind the beam is accounted for by a reduction in the stiffness or modulus. The numerical values to locate the failure point are obtained by the finite element method with thermoplastic stress analysis.

CHAPTER II - STRAIN ENERGY DENSITY THEORY

The strain energy density theory, proposed by G. C. Sih [6-8], is based on the local density of the energy field in an element of material ahead of a high energy concentration area. This theory can predict yielding and/or fracture such that the maxima and the minima of the strain energy density function (dW/dV) corresponds to yielding and fracture respectively. This concept has been applied successfully to a number of engineering problems [5,9,10] since all stressed solids possess minima and maxima of the strain energy density function.

In its general form, the strain energy density function

$$\frac{dW}{dV} = \int_0^{\varepsilon_{ij}} \sigma_{ij} d\varepsilon_{ij} \qquad i,j = 1,2,3 \tag{1}$$

is applicable to elastic or elastic-plastic materials and it reduces to

$$\frac{dW}{dV} = \frac{1}{2} \sigma_{ij}\varepsilon_{ij} \qquad i,j = 1,2,3 \tag{2}$$

for a linear elastic material.

The basic assumptions of the strain energy density theory are:

(1) Yielding and fracture are assumed to coincide with the locations of relative maximum and minimum of the strain energy density function, $(dW/dV)_{max}$ and $(dW/dV)_{min}$, respectively.

(2) The onset of yielding and fracture occur when the maximum of $(dW/dV)_{max}$ and $(dW/dV)_{min}$ reach their respective critical values.

(3) The incremental growth process is governed by

$$\left(\frac{dW}{dV}\right)_c = \frac{S_1}{r_1} = \frac{S_2}{r_2} = \ldots = \frac{S_j}{r_j} = \ldots = \frac{S_c}{r_c} = \text{const.} \tag{3}$$

where S_c and r_c refer to final fracture, Figure 1.

If the process of yielding and/or fracture is approaching global instability, then

$$\begin{aligned} S_1 < S_2 < \ldots < S_j < \ldots < S_c \\ r_1 < r_2 < \ldots < r_j < \ldots < r_c \end{aligned} \tag{4}$$

If the process of yielding and/or fracture is arrested, then

$$\begin{aligned} S_1 > S_2 > \ldots > S_j > \ldots > S_o \\ r_1 > r_2 > \ldots > r_j > \ldots > r_o \end{aligned} \tag{5}$$

where the ratio S_o/r_o replace S_c/r_c in equation (3) such that

$$\left(\frac{dW}{dV}\right)_c = \frac{S_o}{r_o} = \text{const.} \tag{6}$$

When material element yields before fracture, then the energy density dissipated by plastic deformation, $(dW/dV)_p$, is no longer available for release at fracture and it must be subtracted away from $(dW/dV)_c$. The available energy density at fracture is thus

$$\left(\frac{dW}{dV}\right)_c^* = \left(\frac{dW}{dV}\right)_c - \left(\frac{dW}{dV}\right)_p \tag{7}$$

The values of $(dW/dV)_c$ in equations (3) and (6) must then be modified accordingly.

In equation (6), r_o is the radius of the core region which has been estimated by Sih and Kipp [11] theoretically and by Theocaris [12] experimentally. This region represents the resolution of continuum mechanics within which the microstructure of the material becomes influential and must be considered.

This completes the introduction of the strain energy density theory. In what follows, the criterion will be incorporated into the thermoplastic stress analysis.

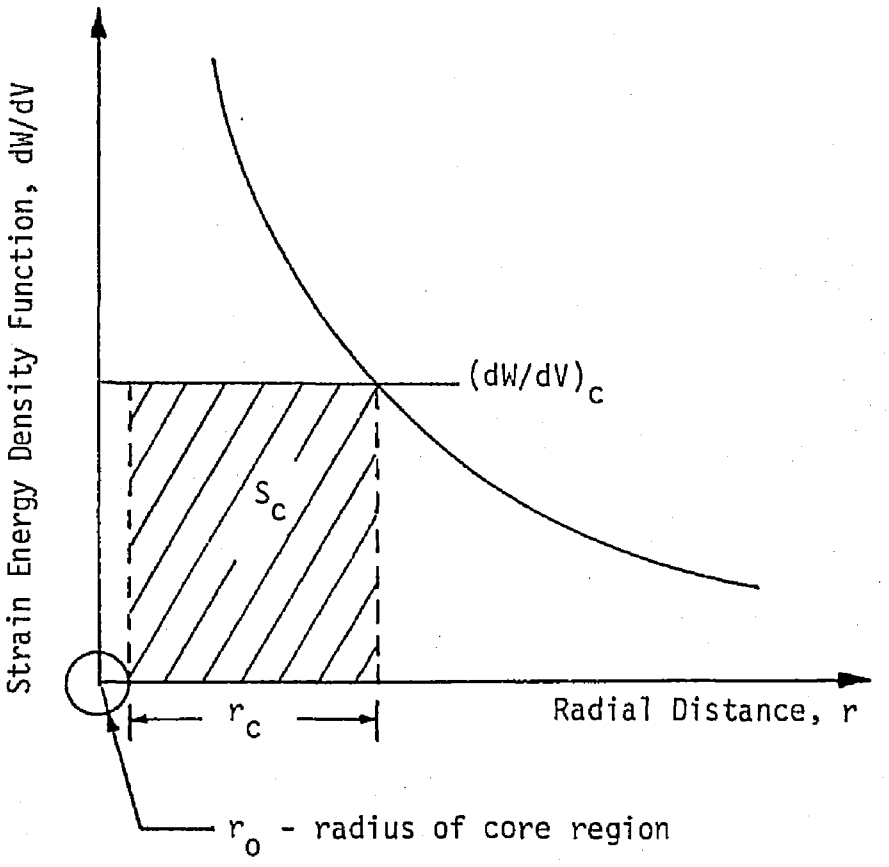

FIGURE 1 - STRAIN ENERGY DENSITY FUNCTION VERSUS RADIAL DISTANCE

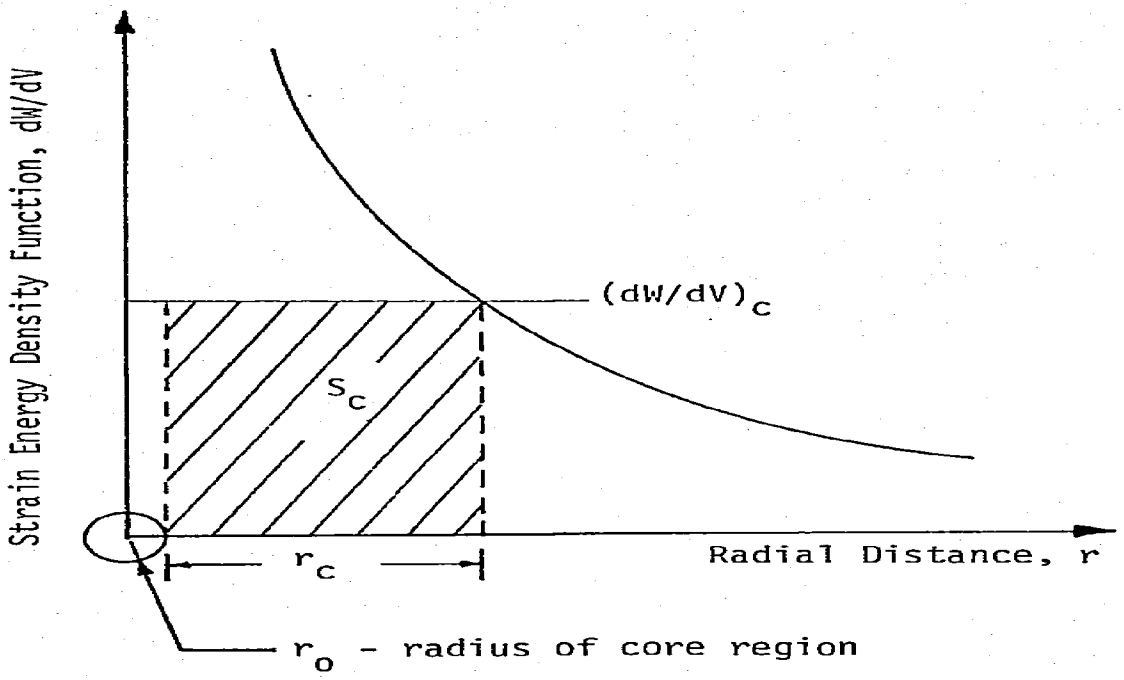

FIGURE 1 - STRAIN ENERGY DENSITY FUNCTION VERSUS RADIAL DISTANCE

CHAPTER III - THERMOPLASTIC STRESS ANALYSIS

The thermoplastic stress analysis is performed by the modified version of PAPST (Plastic Axisymmetric/Planar Structures) computer program which was primarily developed to deal with nonlinear (ductile) fracture problems but it can also be used for thermoelastic and thermoplastic problems. PAPST incorporates a twelve-noded quadrilateral isoparametric element with cubic displacement shape functions. Some of the nonlinear features of PAPST can be stated as follows [13]:

(1) Incremental (flow theory) plasticity with von Mises yield criterion featuring either isotropic or kinematic or a combination of these hardening laws.

(2) Ramberg-Osgood (power hardening) or piecewise linear stress-strain curve description.

(3) Large strain and large displacement formulation.

(4) Newton-Raphson iterative procedure to solve the nonlinear governing equations (tangent stiffness method).

(5) Any number of load-unload-reload cycles to predict mechanically or thermally induced residual stresses and strains.

(6) User-specified load incrementation, with first load increment automatically scaled to first yield.

Depending on the interpolation technique employed, the numerical results for the strain energy density function can show a variation of 10 to 20 percent at the nodes [14]. This can be avoided by contour plotting of dW/dV values at the quadrature points.

Through the use of an updated Lagrangian formulation, finite strain effects are incorporated such that the coordinate system is convected with the deformation. In this convected coordinate system, the relationship between the true strain rate and the deformation rate (or velocity) is unchanged from the small strain theory equations.

Incremental J_2-flow theory of plasticity or von Mises yield criterion is incorporated in PAPST. The deviatoric strain rate components are expressed in terms of the current deviatoric stress components S_{ij} and the components of the deviatoric stress rate $\dot{S}_{ij}$ such that

$$\dot{e}_{ij} = \begin{cases} \frac{1+\nu}{E}\dot{S}_{ij} + \frac{3}{2}f(\sigma_e)S_{ij}\dot{\sigma}'_e & \text{for } \sigma'_e = \sigma_y \text{ and } \dot{\sigma}'_e > 0 \\ \frac{1+\nu}{E}\dot{S}_{ij} & \text{otherwise} \end{cases} \tag{8}$$

where

$$\dot{e}_{ij} = \dot{\varepsilon}_{ij} - \frac{1}{3}\dot{\varepsilon}_{pp}\delta_{ij}$$

$$S_{ij} = \sigma_{ij} - \frac{1}{3}\sigma_{pp}\delta_{ij}$$

$$\sigma_e = \sqrt{\frac{3}{2} S_{ij} S_{ij}}$$

$$\sigma'_e = \sqrt{\frac{3}{2} S'_{ij} S'_{ij}} \qquad (9)$$

The above quantities are defined as follows:

$\dot{e}_{ij}$ = the deviatoric strain rate components

S_{ij} = the current deviatoric stress components

S'_{ij} = the deviatoric stress components measured from the center of the current yield surface

$f(\sigma_e)$ = a function dependent on the uniaxial stress-strain curve as described subsequently

σ_e = von Mises effective stress

σ'_e = von Mises effective stress with respect to the coordinates of the current center of the yield surface

σ_y = yield stress

a_{ij} = the coordinates in stress space of the center of the yield surface.

The coordinates of the center of the yield surface, a_{ij}, are given by

$$a_{ij} = \begin{cases} \frac{3}{2} \beta S'_{k\ell} S'_{ij} / \sigma'^2_e & \text{for } \sigma'_e = \sigma_y \text{ and } \sigma'_e > 0 \\ 0 & \text{otherwise} \end{cases} \tag{10}$$

where β is related to the hardening laws such that $\beta = 0$ corresponds to isotropic hardening and $\beta = 1$ to kinematic hardening while $0<\beta<1$ represents combined hardening.

Figure 2(a) shows isotropic hardening where the yield surface expands uniformly about the origin. Figure 2(b) is that of kinematic hardening where the yield surface translates as a rigid body. Combined hardening of Figure 2(c) is the case where the yield surface both expands and translates.

The function $f(\sigma_e)$ in equation (8) is defined [13]

$$f(\sigma_e) = \frac{\dot{\varepsilon}^p}{\sigma_e \dot{\sigma}_e} \tag{11}$$

This function depends on the mathematical model used to represent the stress-strain curve. The stress-strain curve is approximated by using a bilinear model. The following relationship is used:

$$\varepsilon = \frac{\sigma}{E} + \frac{\alpha}{E} (\sigma - \sigma_y) \tag{12}$$

The plastic strain rate is given by

$$\dot{\varepsilon}_{plastic} = \frac{\alpha\dot{\sigma}_e}{E} \tag{13}$$

which together with equation (11) gives

$$f(\sigma_e) = \frac{\alpha}{E\sigma_e} \tag{14}$$

where α, E are user specified and σ_e is the current value of the effective stress.

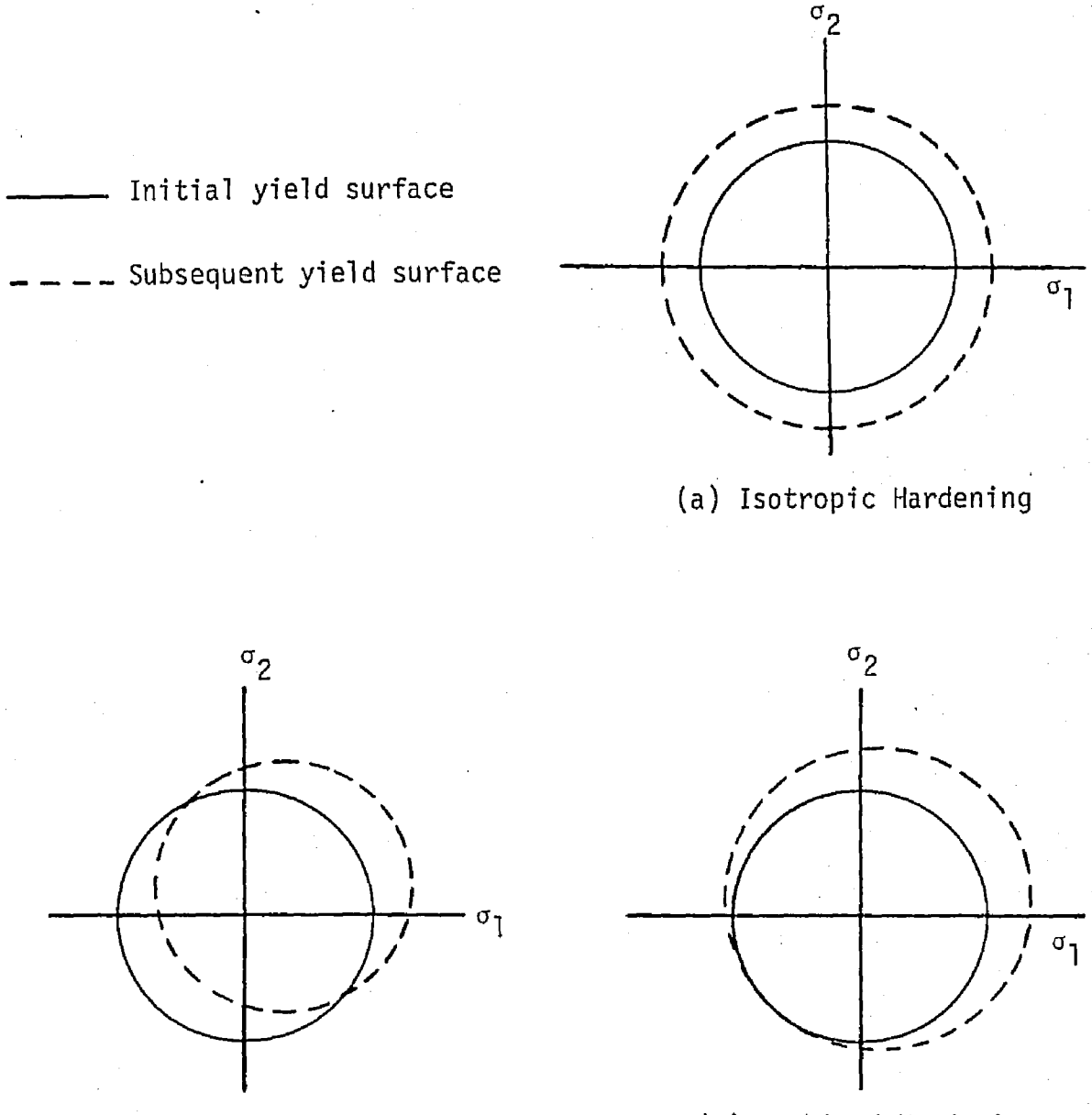

FIGURE 2 - DIAGRAMS OF HARDENING MODELS

CHAPTER IV - ITERATIVE SOLUTION BY FINITE ELEMENT

The finite element method is used to approximate the governing equations of the incremental thermoplasticity. These equations are of the form:

$$\underset{\sim}{K}(\underset{\sim}{u}) \cdot \dot{\underset{\sim}{u}} - \dot{\underset{\sim}{R}} = 0 \tag{15}$$

where $\dot{\underset{\sim}{R}}$ is the nodal loading rate vector and $\dot{\underset{\sim}{u}}$ the corresponding nodal velocity vector. The stiffness matrix is given by

$$[\underset{\sim}{K}(\underset{\sim}{u})] = \sum_{\text{elements}} \int_{\text{element area}} \underset{\sim}{B}^T \underset{\sim}{D}(\underset{\sim}{u}) \underset{\sim}{B} dA \tag{16}$$

and it depends on the current nodal displacement vector through the matrices $[\underset{\sim}{D}(\underset{\sim}{u})]$ and $[\underset{\sim}{B}(\underset{\sim}{u})]$ in which $[\underset{\sim}{D}(\underset{\sim}{u})]$ relates the stress and strain rates and $[\underset{\sim}{B}(\underset{\sim}{u})]$ the strain rate to nodal displacement rate. Equations (15) are then integrated over one load increment at a time to determine the nodal displacements, $\underset{\sim}{u}$, by making use of the Newton-Raphson technique.

Convergence criteria are based on the comparison of the following three factors [15]:

(1) The mean square of the residual force vector

$$|F|^2 = \underset{\sim}{F} \cdot \underset{\sim}{F} \tag{17}$$

which enforces equilibrium

(2) The mean square of the increment load vector

$$|\Delta R|^2 = \Delta \underset{\sim}{R} \cdot \Delta \underset{\sim}{R} \tag{18}$$

(3) The total load vector for the particular increment

$$|R|^2 = \underset{\sim}{R} \cdot \underset{\sim}{R} \tag{19}$$

The comparison gives the user specified convergence values such that

$$\frac{|F|^2}{|\Delta R|^2} \leq C_1 = 0.05 \quad \text{(increment equilibrium)} \tag{20}$$

$$\frac{|F|^2}{|R|^2} \leq C_2 = 10^{-7} \quad \text{(overall equilibrium)} \tag{21}$$

CHAPTER V - ANALYTICAL MODELING AND MATERIAL PROPERTIES

Figure 3 shows a laser beam traveling across the plate. The plate is 7075-T651 aluminum with a thickness of 0.635 cm. The applied mechanical stress is 2.179×10^2 MPa. The laser beam is traveling from left to right at a speed of 63.5 cm/sec and it has a radius of 1.65 cm. The intensity of the laser beam is 1.4 kW/cm^2. It is assumed that within that radius, the temperature is well above the melting point of the material (540°C) and is distributed uniformly. Experiments* have shown that the laser beam evaporates about one third of the material in the thickness direction (0.23 cm). The problem, in general, is three-dimensional in character. However, depending on the nature of loading, certain simplifications are introduced. For example, the bending due to the notch shaped plate behind the laser beam will be neglected since it is found to be relatively small.

The temperature distribution around a moving point heat source is [4]

$$T(\xi_1,\xi_2) = \frac{Q_0}{2\pi\kappa h} e^{-\sigma\xi_1} K_0(\sigma r) \tag{22}$$

where

$$r = \sqrt{\xi_1^2+\xi_2^2} \text{ and } \sigma = \frac{v}{2\kappa},\ \kappa = \frac{k}{\rho c} \tag{23}$$

*Information supplied by the Naval Research Laboratory.

Defined are the quantities:

Q_o = magnitude of the heat source

v = velocity of the source

κ = thermal diffusivity

k = thermal conductivity coefficient

ρ = mass density

c = specific heat

h = thickness

ξ_1, ξ_2 = moving coordinate system

Equation (22) is modified by using Green's function to give the temperature distribution around a circular moving laser beam as shown in Appendix A.

Figure 3 also shows the two distinct zones with different material properties. Zone 1 is the base material and zone 2 is the laser damaged area. Loss in material integrity is modeled by reduction in the yield strength and elastic modulus. This is shown by the difference in material properties of the two different zones in Table 1.

A bilinear material model is used with γ determining the slope of the strain hardening line

$$\varepsilon = \begin{cases} \sigma/E + \alpha T & \text{for } \sigma \leq \sigma_y \\ \frac{\sigma}{E}(1+\gamma) - \gamma\frac{\sigma_y}{E} + \alpha T & \text{for } \sigma > \sigma \end{cases} \tag{24}$$

TABLE 1 - MATERIAL PROPERTIES

	Zone 1	Zone 2
σ_y (MPa)	2.179×10^2	6.895×10^1
E (MPa)	7.171×10^4	6.895×10^2 ($E_{effective}$)
α (1/°C)	0.0000239	0.0000240
ν	0.33	0.33

and the slope of the strain hardening line is given by

$$\frac{d\sigma}{d\varepsilon} = \frac{E}{1+\gamma} \text{ with } \gamma = 10 \tag{25}$$

Care must be taken in the calculation of the strain energy density function, dW/dV, since it is the area under the stress-strain curve and the thermal strains do not contribute as shown in Figure 4.

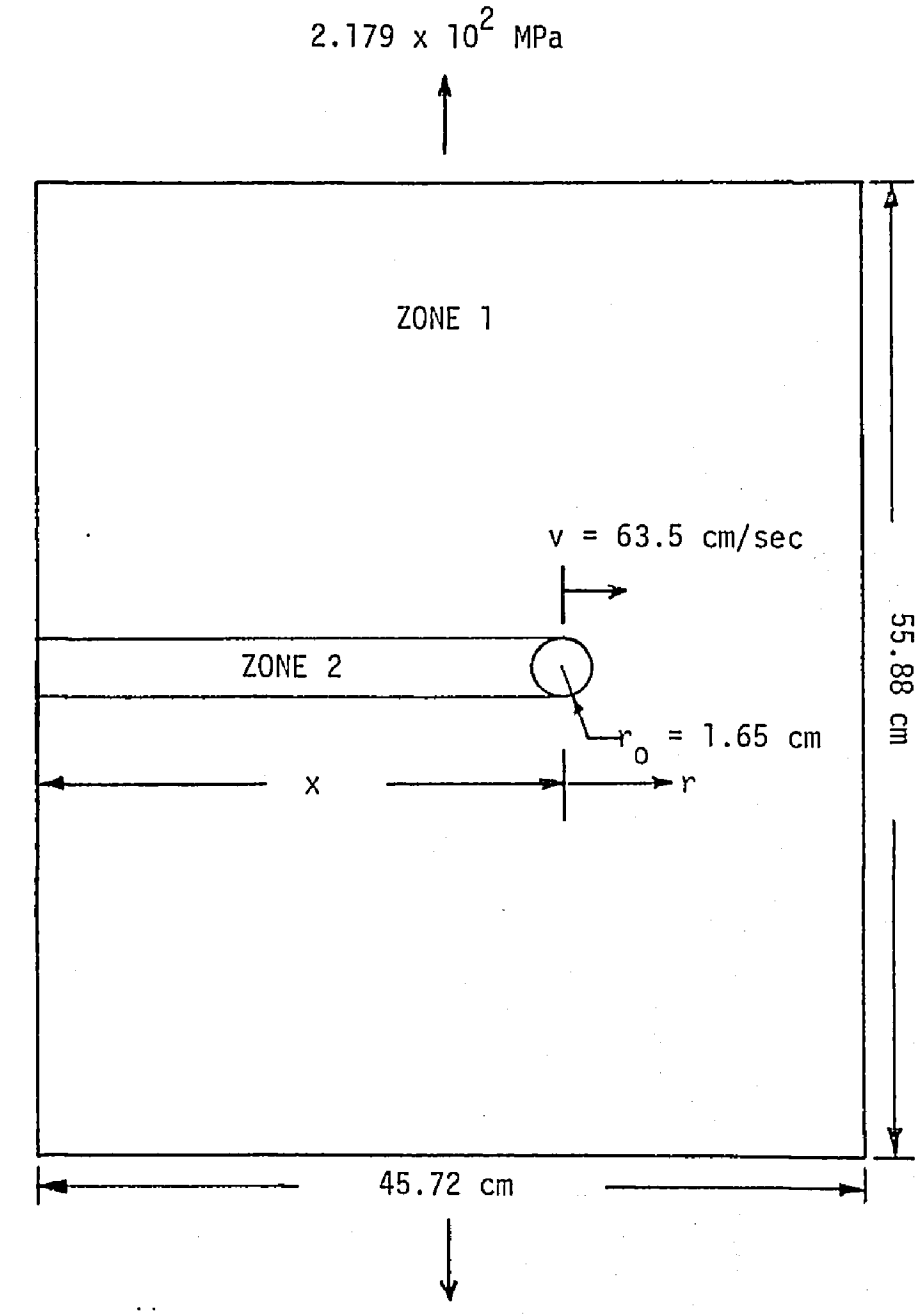

FIGURE 3 - PLATE SUBJECTED TO A MOVING LASER BEAM AND A TENSILE LOAD

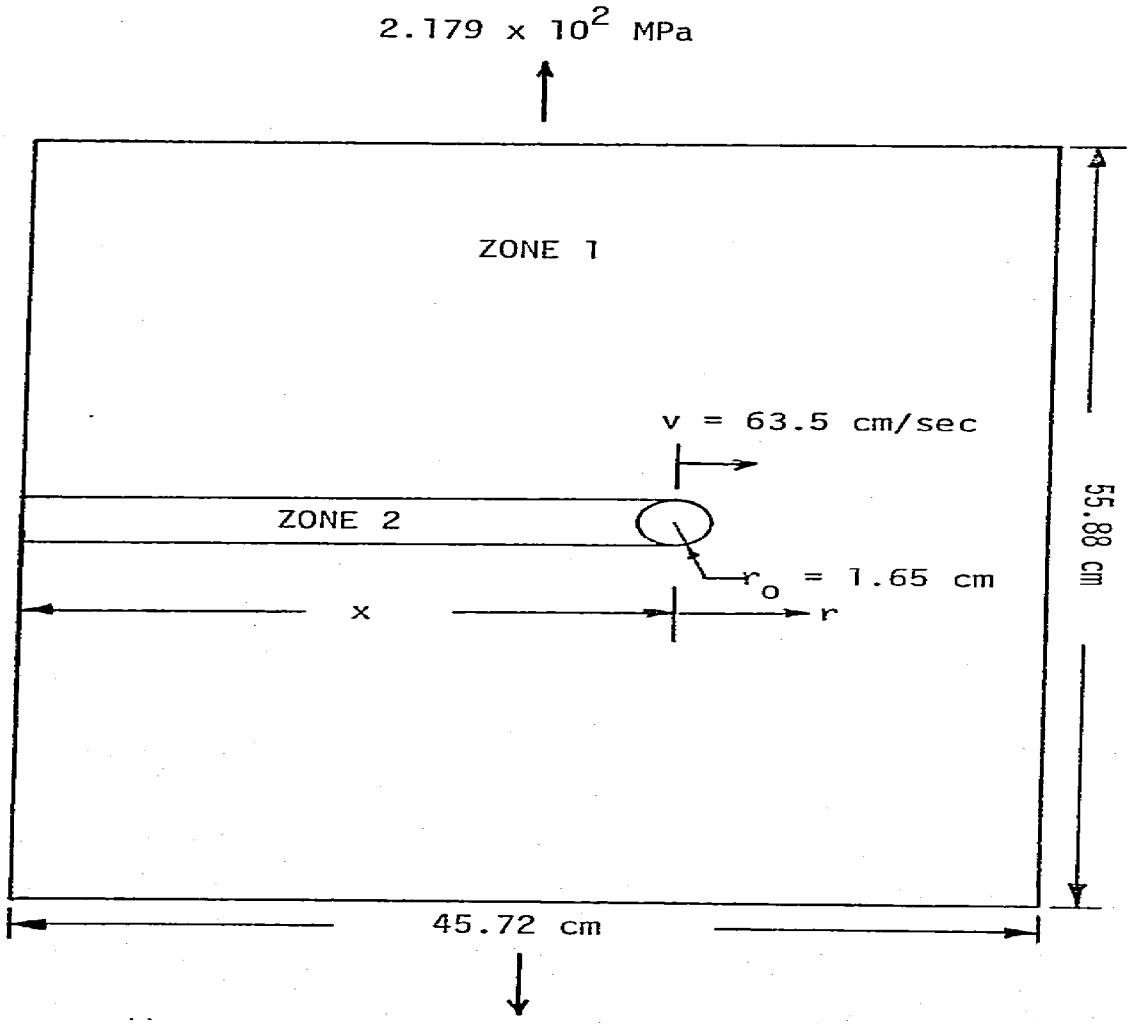

FIGURE 3 - PLATE SUBJECTED TO A MOVING LASER BEAM AND A TENSILE LOAD

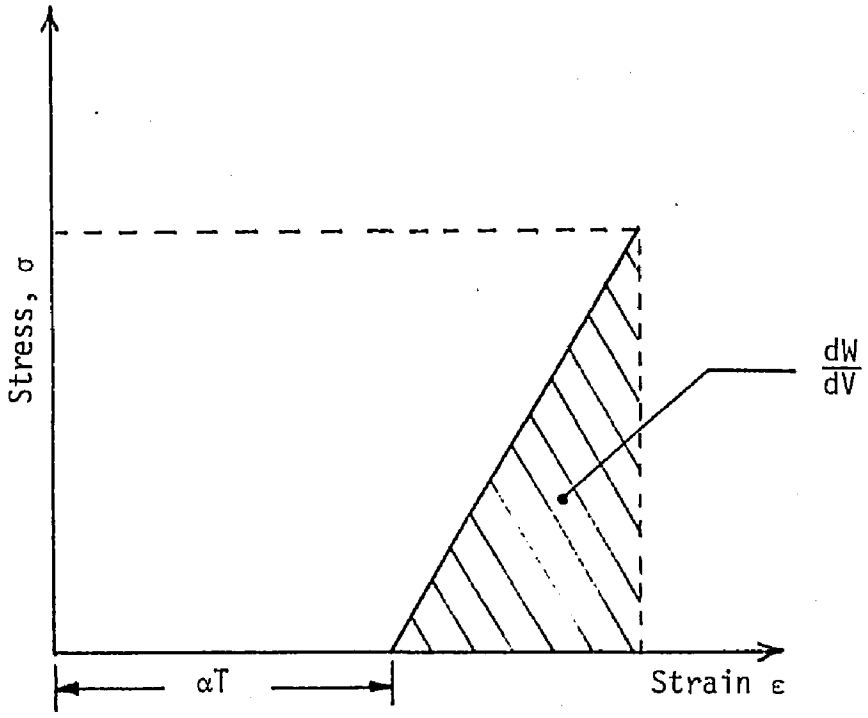

FIGURE 4 - STRESS, THERMAL STRAIN, MECHANICAL STRAIN AND (dW/dV)

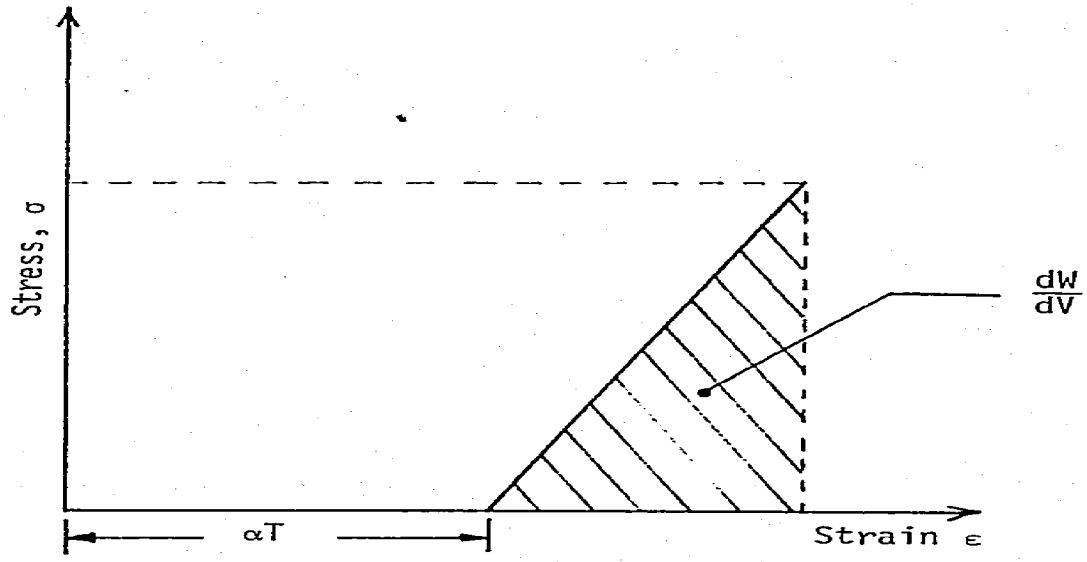

FIGURE 4 - STRESS, THERMAL STRAIN, MECHANICAL STRAIN AND (dW/dV)

CHAPTER VI - DISCUSSION OF RESULTS

The finite element grid patterns for the laser beam traveling from left to right are shown in Figures 5 through 16. They are all subjected to tensile loading of 2.179×10^2 MPa. Starting from the edge of the plate, the laser beam is moved incrementally at constant step of 2.54 cm for a total of twelve (12) increments. The deformation of the plate is cumulated while the material behind the laser is damaged such that the undamaged ligament experiences more and more bending as the laser beam covers more ground. The effective stresses and strain energy density functions are computed for each increment of laser beam movement so that material damage at each step can be evaluated.

Referring to Figures 17 to 20, the effective stress (σ_e) contours are plotted for laser beam traversed to distances of x = 7.62, 15.24, 22.86 and 27.94 cm as referenced from the plate edge shown in Figure 3. The material near the laser source acquires higher yield intensity. Refer to the contours 7, 8 and 9 in Figure 17. The value of σ_e for contour 9 is beyond the yield strength. Note that the intensity drops substantially at the trailing path of the beam corresponding to contour 1. The amount of yielding increases with the laser path. This is evidenced by the fact that yielding corresponds to contour 7 in Figure 18 and contour 5 in Figure 19. When x = 27.94 cm, yielding covers more than one third of the plate and the plate reaches the critical condition of global instability according to the strain energy density criterion. The numbering of the finite element grid pat-

tern for x = 27.94 cm can be found in Figure 21.

Contours of constant strain energy density are displayed in Figures 22 through 25 when the laser beam is at x = 27.94 cm from the left reference point. Each of Figures 22 through 25 shows the strain energy density contours in a different element of Figure 21 as indicated in Table 2.

TABLE 2 - REFERENCE OF FINITE ELEMENT POSITION IN FIGURES 22 TO 25

Figure No.	Element No.
22	5
23	9
24	14
25	19 and 24

Refer to finite element position in Figures 22 through 25. For a constant radius of r, Figures 22 through 24 show the variation of the strain energy density with respect to the polar angle θ. The minimum value of the strain energy density always occurs at $\theta = 0°$ and the maximum at $\theta = 180°$. This observation is in perfect agreement with the first assumption of the strain energy density theory since fracture and yielding are predicted to occur at $\theta = 0°$ and at $\theta = 180°$, respectively.

When the strain energy density dW/dV is examined as a function of r ($\theta = 0°$), the values of dW/dV first decrease and then increase with

increasing r. Table 3 displays the values of dW/dV as a function of r where the minimum is around the critical $(dW/dV)_c^* = 2.283\ MJ/m^3$.

TABLE 3 - STRAIN ENERGY DENSITY VALUES AHEAD OF THE LASER BEAM*

Distance from the Center of the Laser Beam (cm)	Distance from the Left Reference Point (cm)	dW/dV (MJ/m^3)
8.04	35.98	4.40
9.74	37.68	3.37
11.43	39.37	2.26
13.55	41.49	5.94
15.66	43.60	1.58×10^1
17.78	45.72	2.72×10^1

The difference between $(dW/dV)_c$ and $(dW/dV)_c^*$ is given in equation (7). One important fact to be reminded as mentioned earlier is that the numerical results for dW/dV at the nodes can vary from 10 to 20%. However, it is obvious that the minimum is around $(dW/dV)_c^*$ and that its location is approximately 39.37 cm from the left reference point. The prediction of this failure location tends to agree with the experimental observation.

Figure 25 shows the strain energy density function dW/dV in elements 19 and 24 where the location of the minimum can be observed in

*These are the values corresponding to the case when the laser beam is 27.94 cm away from the left reference point.

contour forms.

In Appendix B, listed are the strain energy density values as a function of r ($\theta = 0°$) at x = 7.62, 15.24 and 22.86 cm for comparison purposes. For the cases of x = 7.62 and 15.24 cm (Tables 4 and 5), the strain energy density values are decreasing for increasing r. At x = 22.86 cm (Table 6), dW/dV first decrease and then increase for increasing r. It is this minimum that reaches $(dW/dV)_c^*$ value at x = 27.94 cm (Table 3). Tables 3 through 6, by comparison, reveals that more and more energy is inputted for increasing x which takes the plate up to the point of global instability.

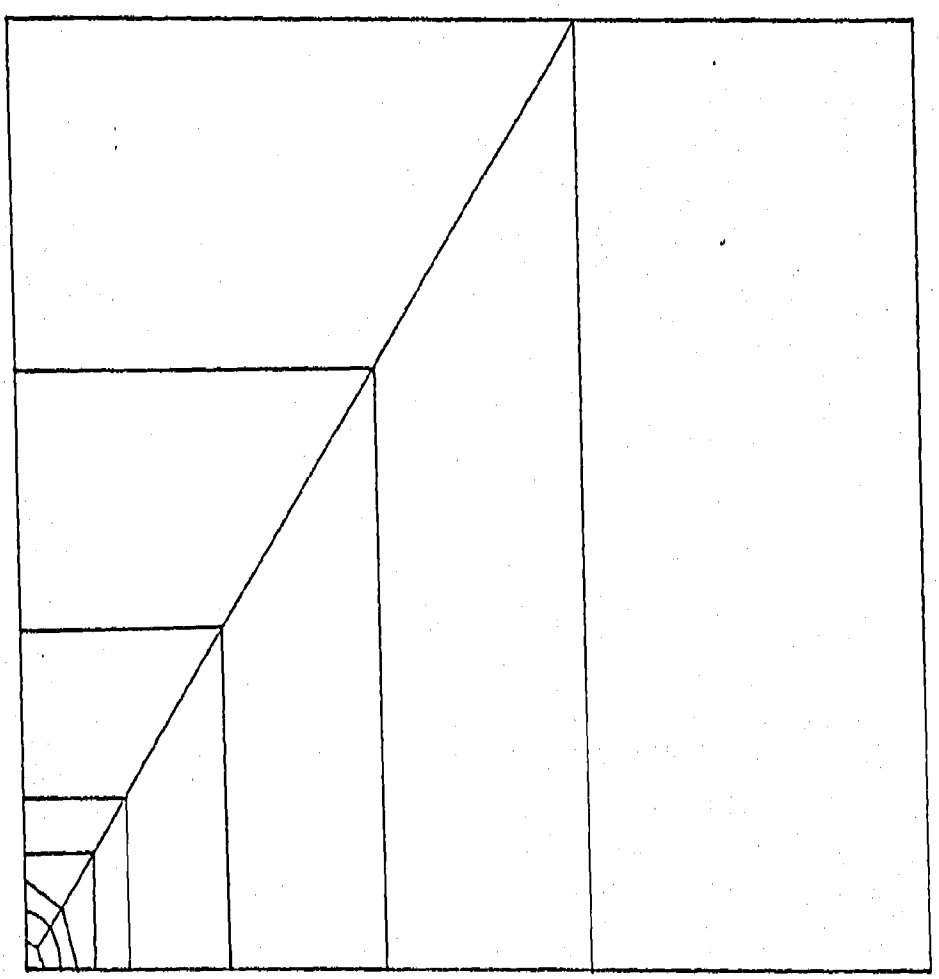

FIGURE 5 - FINITE ELEMENT GRID PATTERN FOR x = 0.0 cm

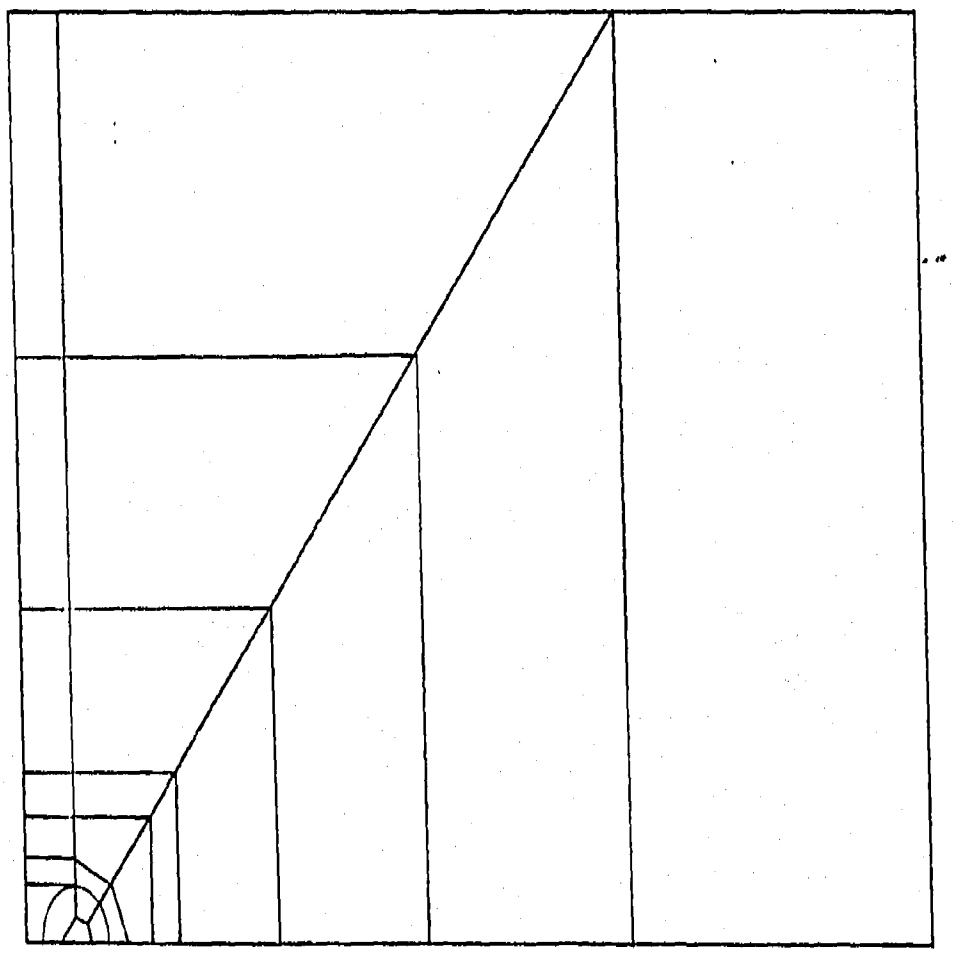

FIGURE 6 - FINITE ELEMENT GRID PATTERN FOR x = 2.54 cm

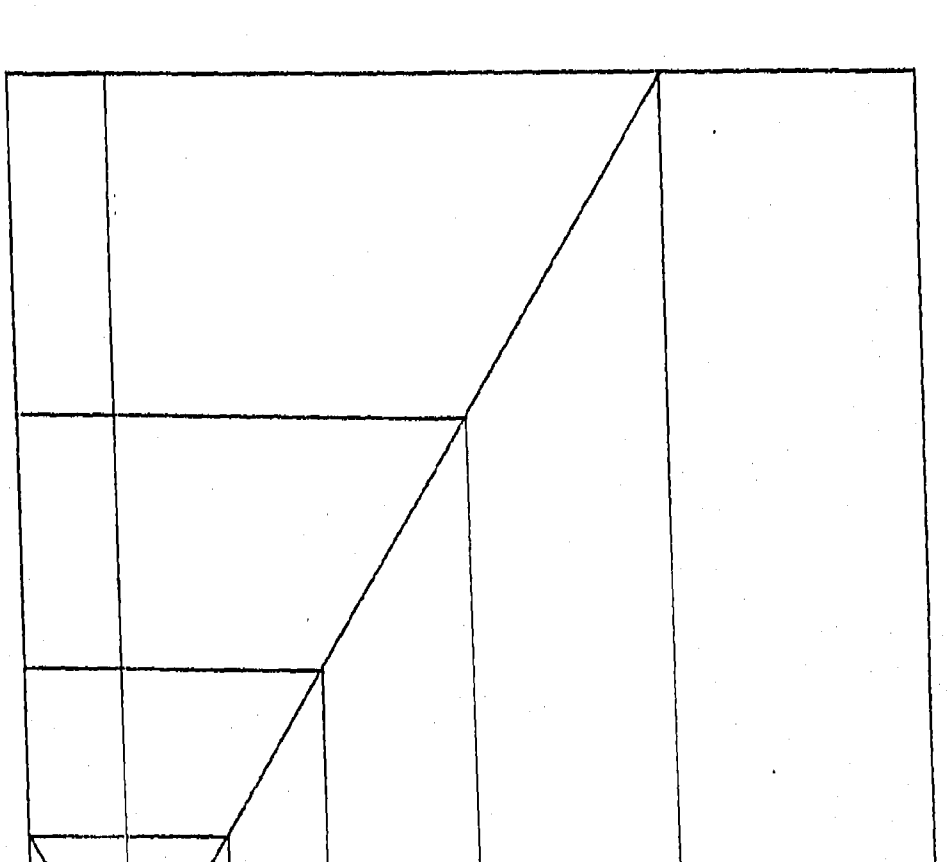

FIGURE 7 - FINITE ELEMENT GRID PATTERN FOR x = 5.08 cm

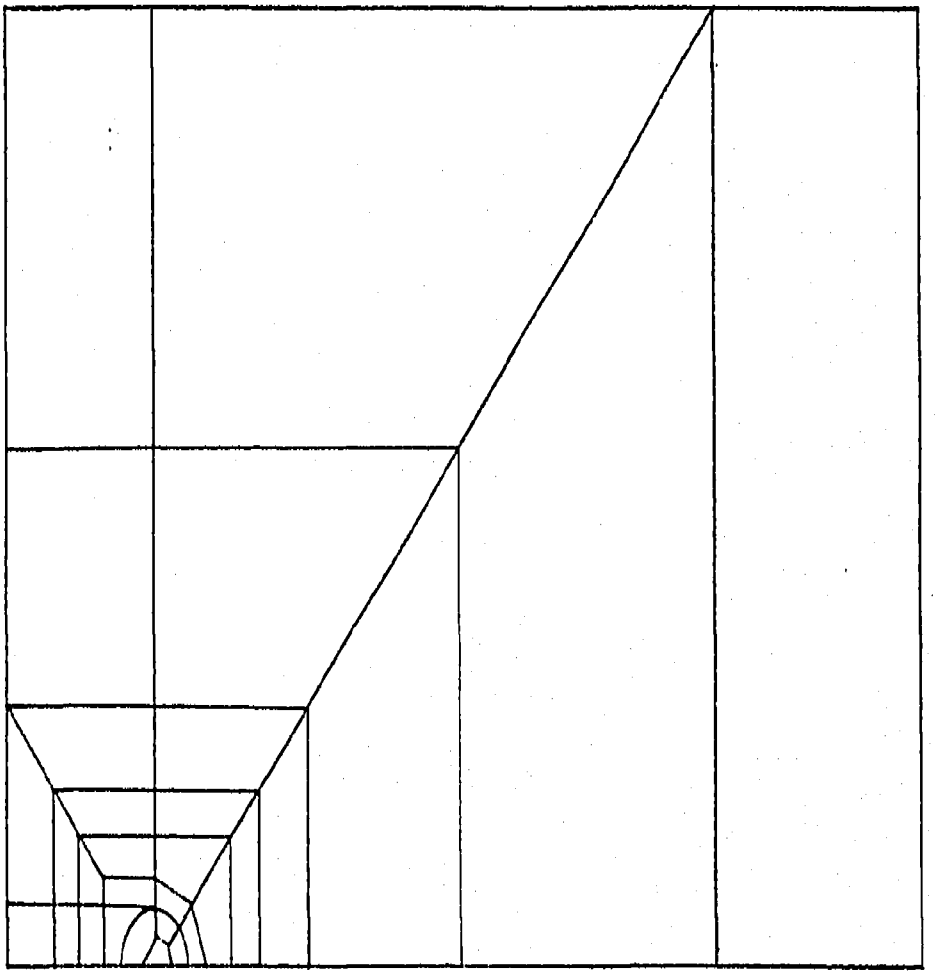

FIGURE 8 - FINITE ELEMENT GRID PATTERN FOR x = 7.62 cm

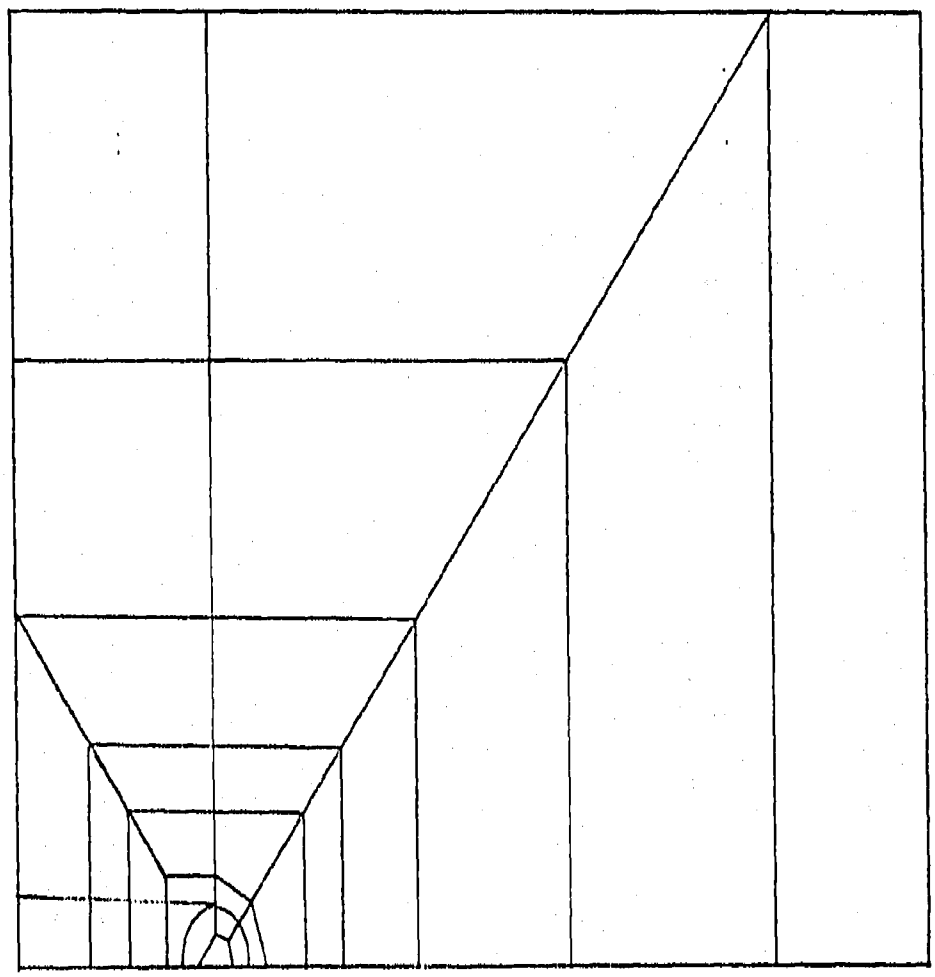

FIGURE 9 - FINITE ELEMENT GRID PATTERN FOR x = 10.16 cm

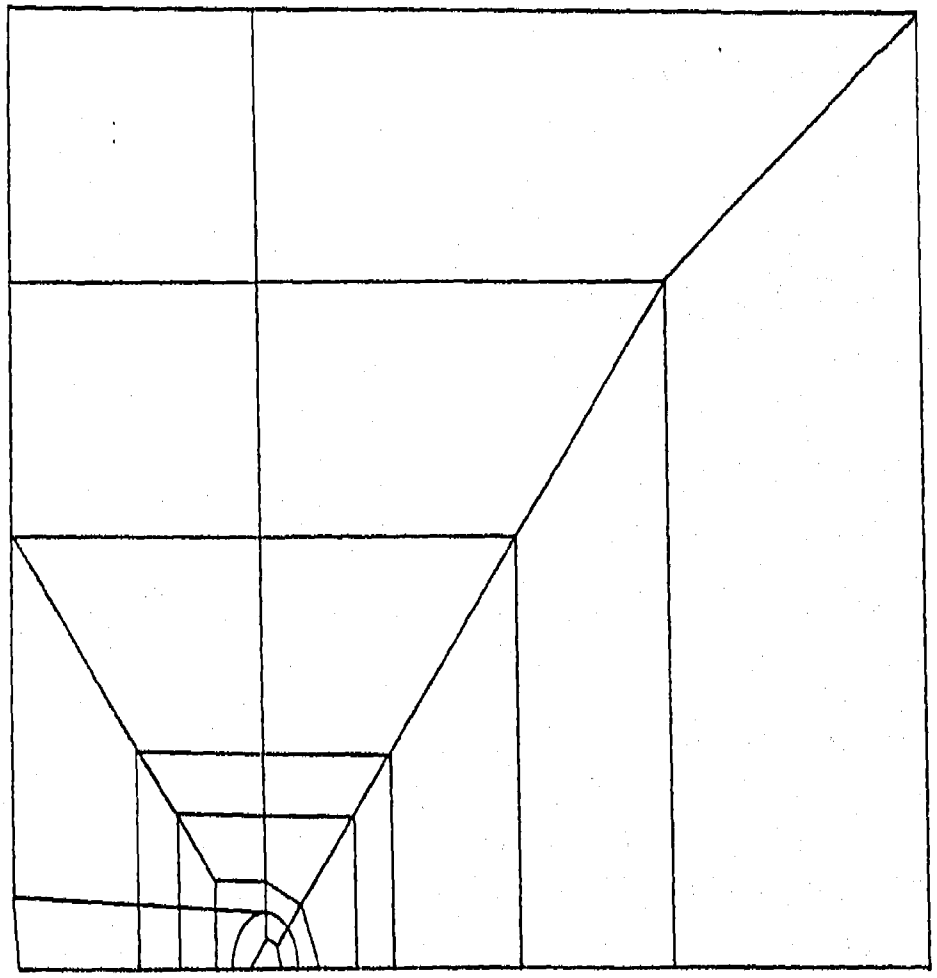

FIGURE 10 - FINITE ELEMENT GRID PATTERN FOR x = 12.70 cm

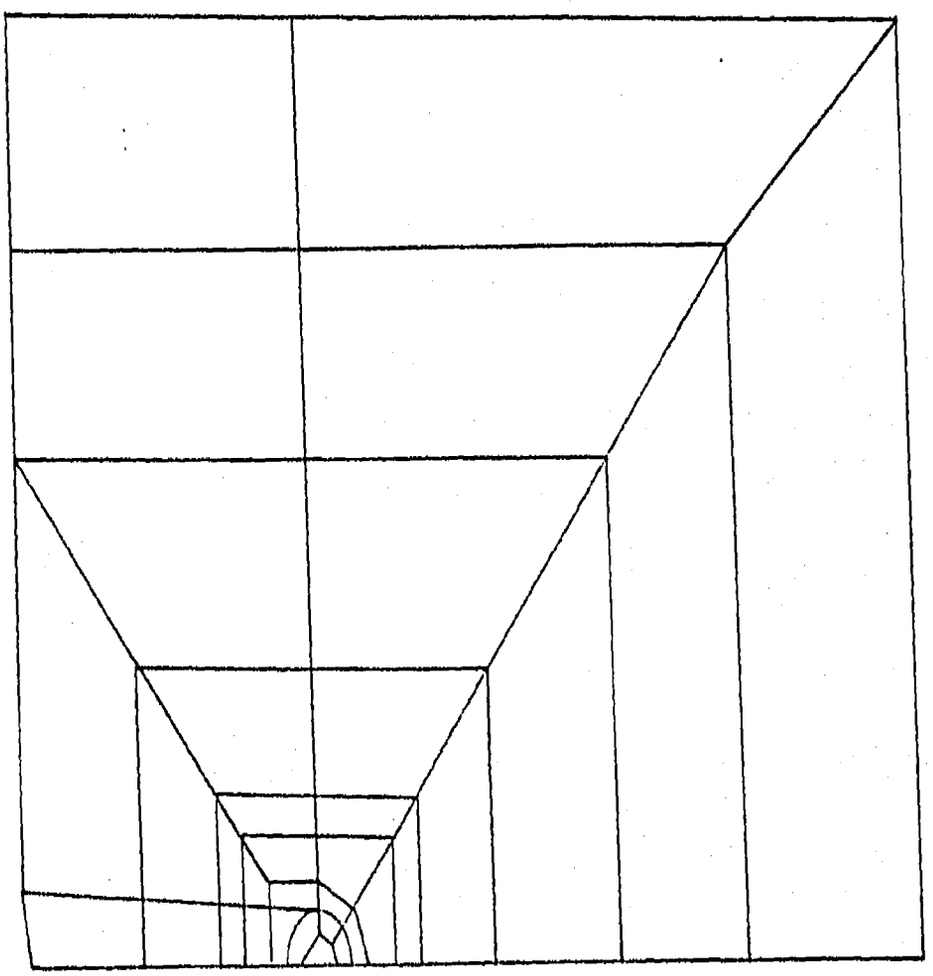

FIGURE 11 - FINITE ELEMENT GRID PATTERN FOR x = 15.24 cm

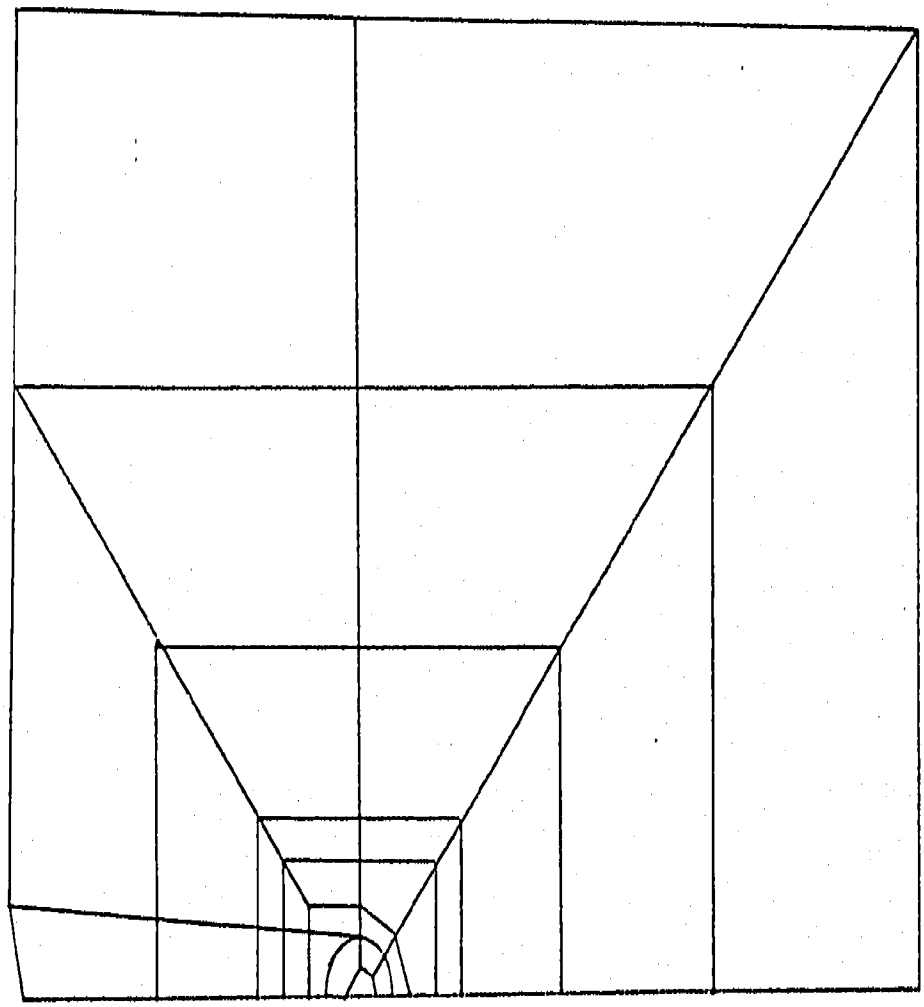

FIGURE 12 - FINITE ELEMENT GRID PATTERN FOR x = 17.78 cm

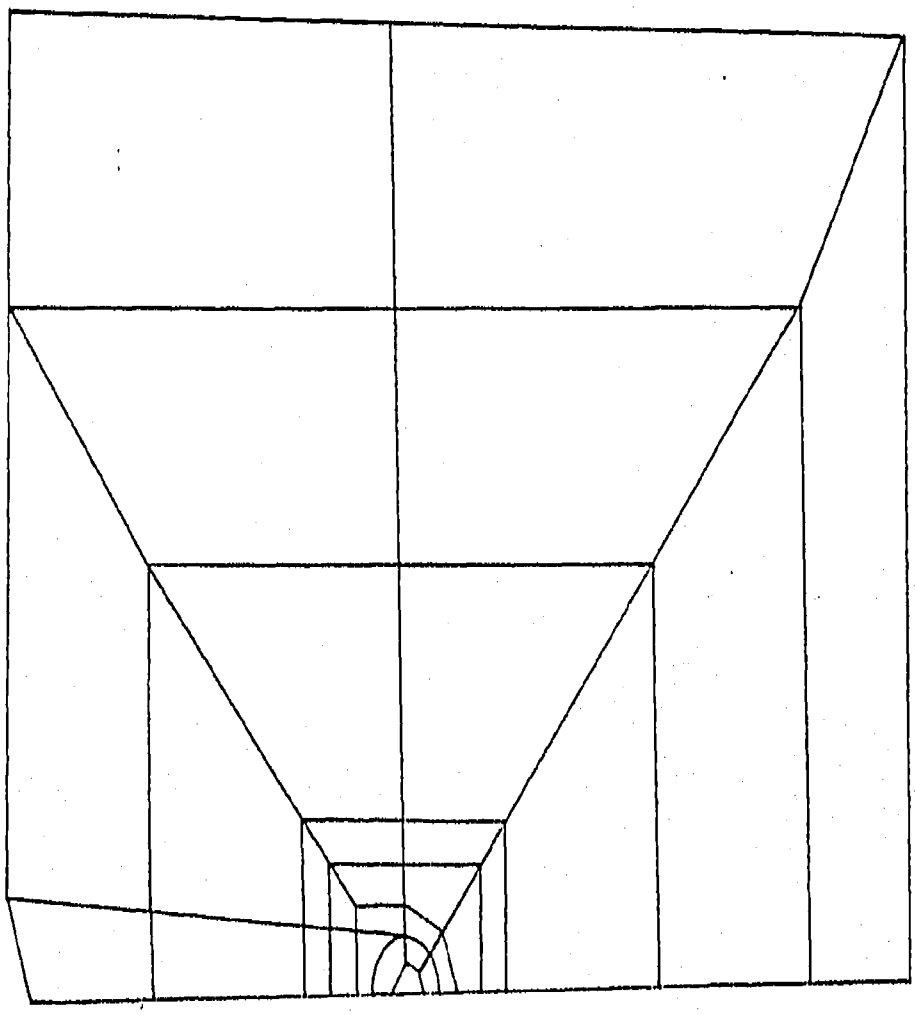

FIGURE 13 - FINITE ELEMENT GRID PATTERN FOR x = 20.32 cm

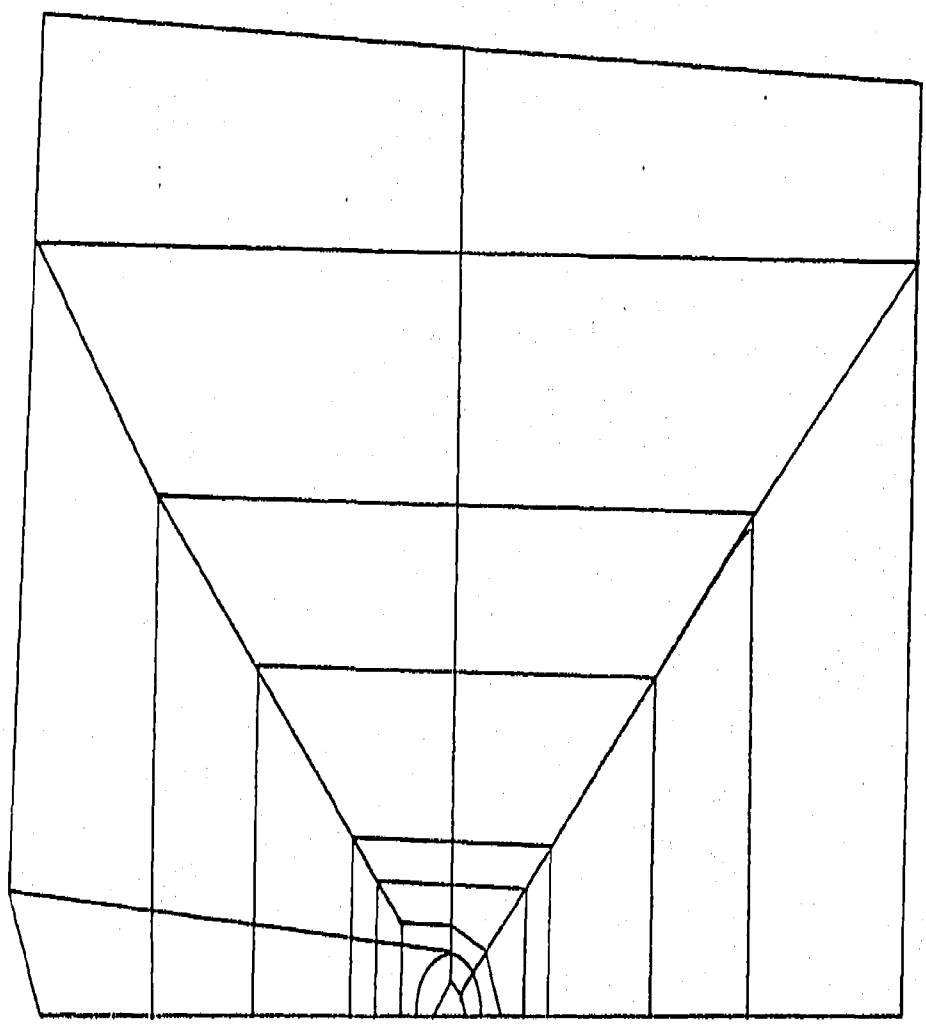

FIGURE 14 - FINITE ELEMENT GRID PATTERN FOR x = 22.86 cm

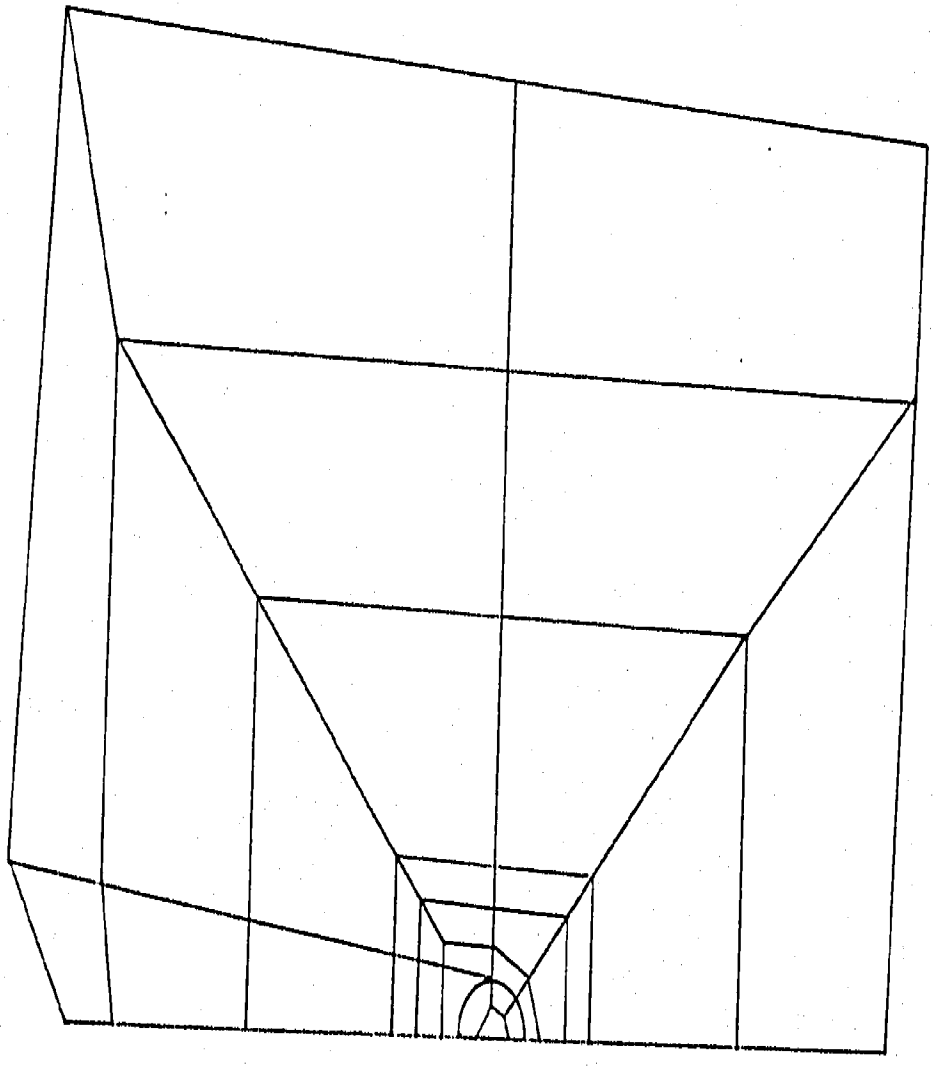

FIGURE 15 - FINITE ELEMENT GRID PATTERN FOR x = 25.40 cm

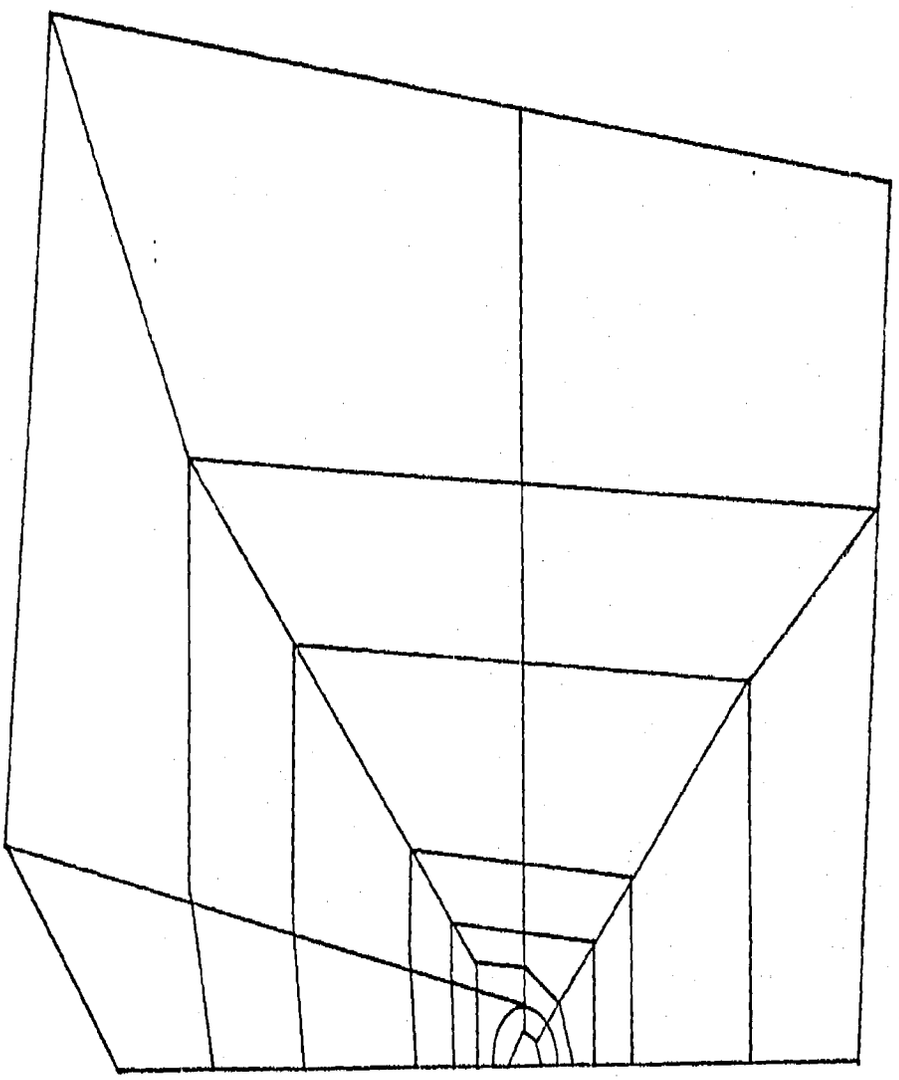

FIGURE 16 - FINITE ELEMENT GRID PATTERN FOR x = 27.94 cm

CONTOUR VALUES (MPa)

1 - 3.723×10^{1}	4 - 1.724×10^{2}	7 - 2.551×10^{2}
2 - 8.963×10^{1}	5 - 1.999×10^{2}	8 - 3.103×10^{2}
3 - 1.448×10^{2}	6 - 2.275×10^{2}	9 - 4.757×10^{2}

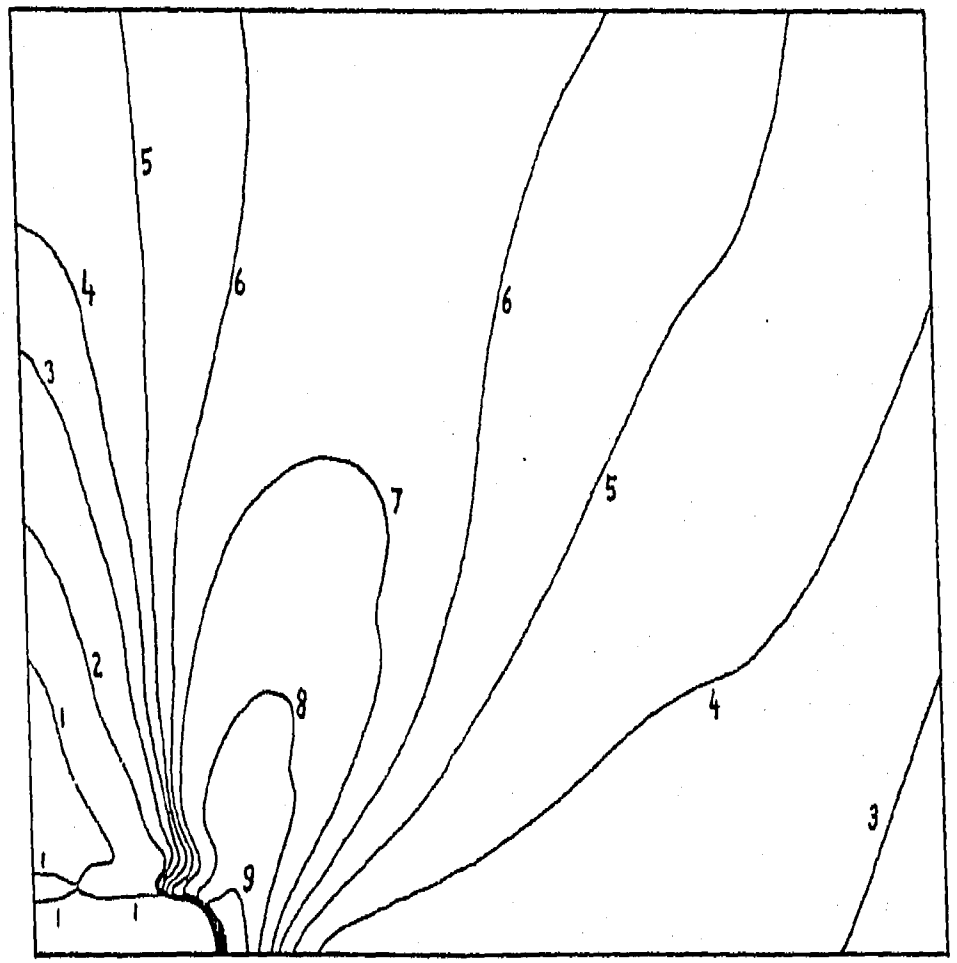

FIGURE 17 - EFFECTIVE STRESS CONTOURS FOR x = 7.62 cm

CONTOUR VALUES (MPa)

1 - 5.378×10^{1}

2 - 1.172×10^{2}

3 - 1.862×10^{2}

4 - 2.551×10^{2}

5 - 3.172×10^{2}

6 - 3.861×10^{2}

7 - 4.757×10^{2}

8 - 5.171×10^{2}

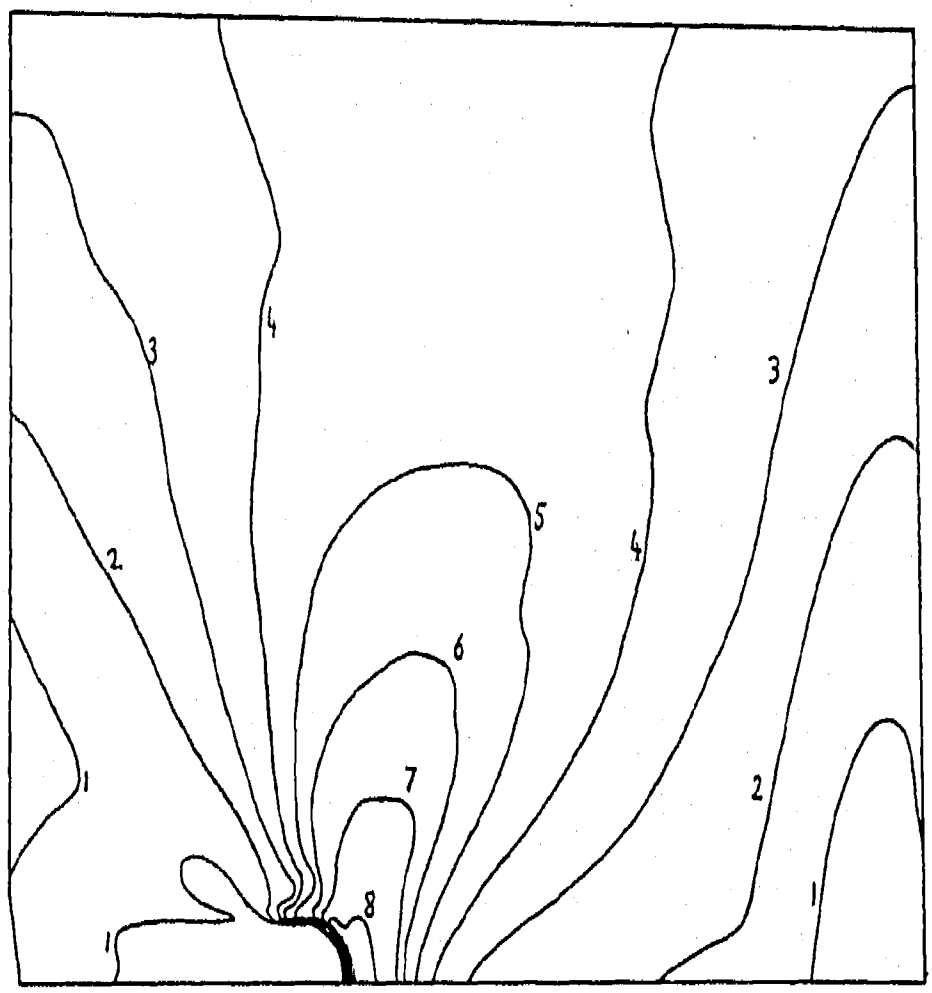

FIGURE 18 - EFFECTIVE STRESS CONTOURS FOR x = 15.24 cm

CONTOUR VALUES (MPa)

1 - 8.963×10^{1}

2 - 1.793×10^{2}

3 - 2.689×10^{2}

4 - 3.585×10^{2}

5 - 4.757×10^{2}

6 - 5.378×10^{2}

7 - 5.792×10^{2}

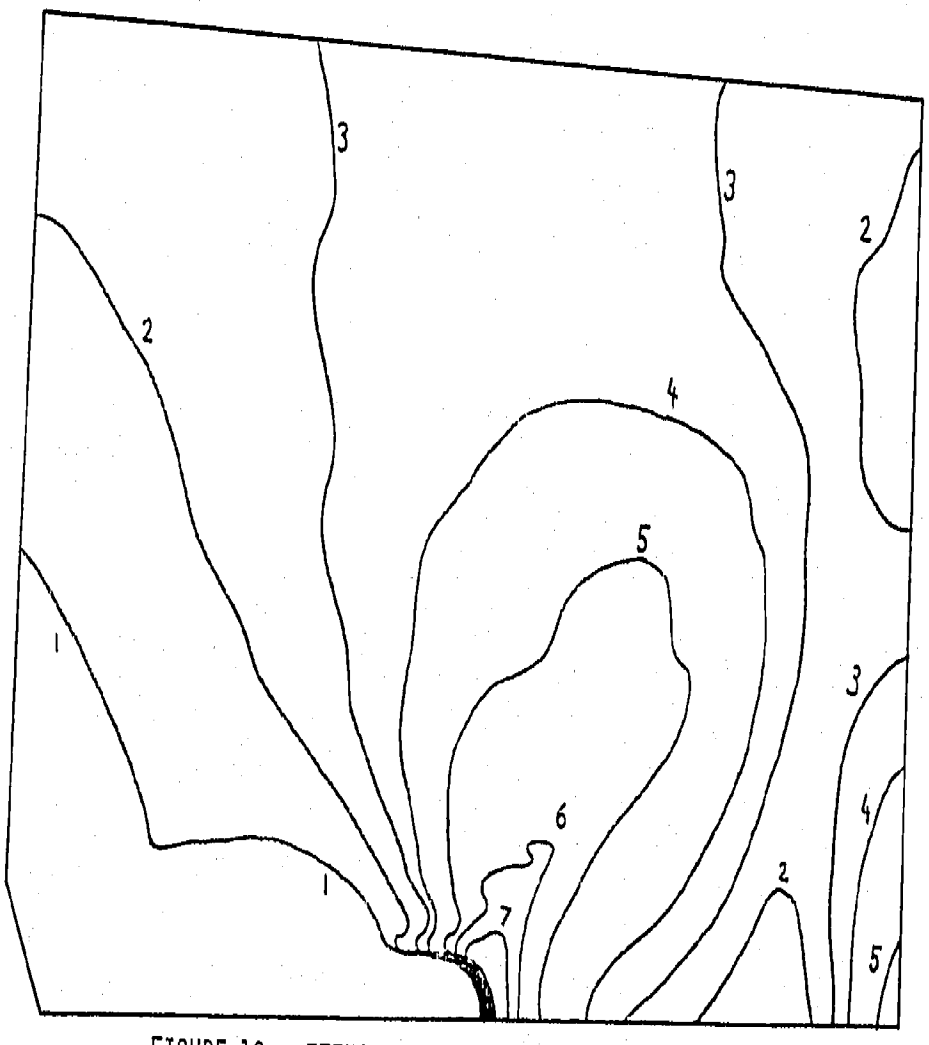

FIGURE 19 - EFFECTIVE STRESS CONTOURS FOR x = 22.86 cm

CONTOUR VALUES (MPa)

1 - 1.310×10^2	4 - 3.792×10^2	7 - 6.274×10^2
2 - 2.137×10^2	5 - 4.757×10^2	8 - 7.584×10^2
3 - 2.965×10^2	6 - 5.447×10^2	

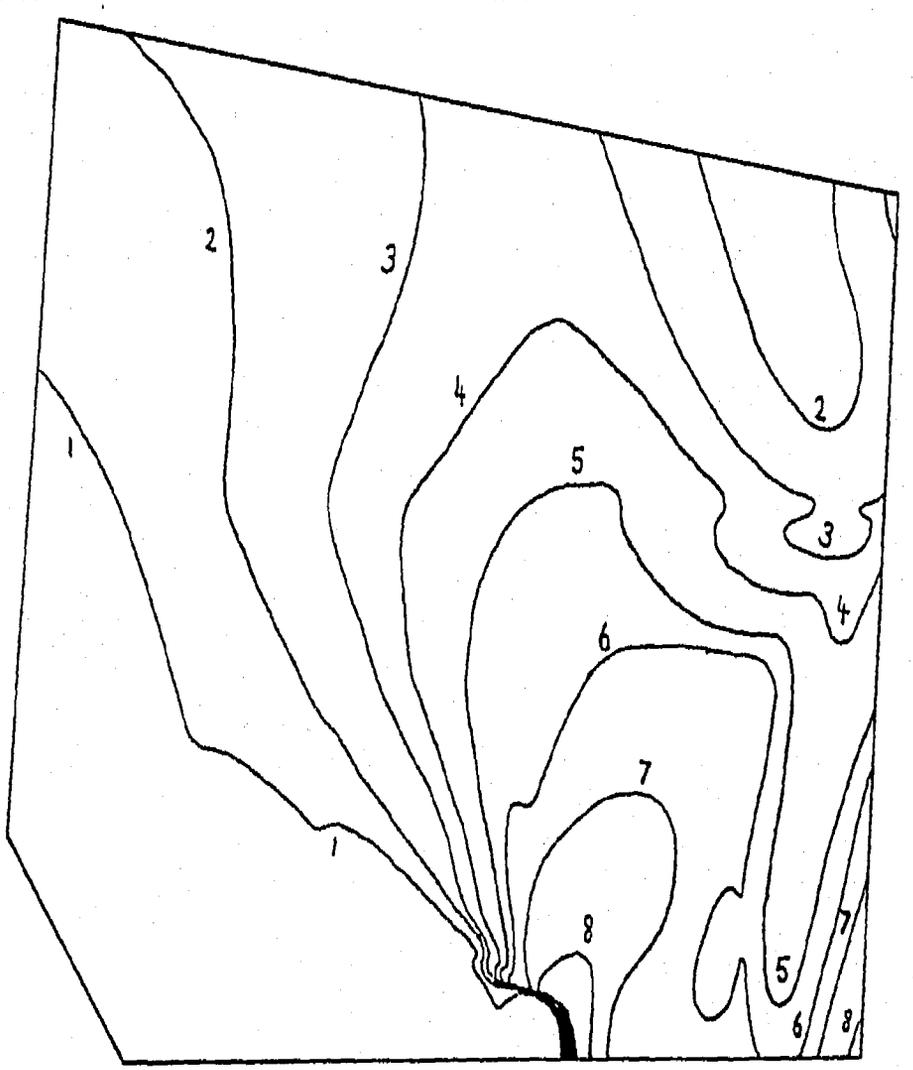

FIGURE 20 - EFFECTIVE STRESS CONTOURS FOR x = 27.94 cm

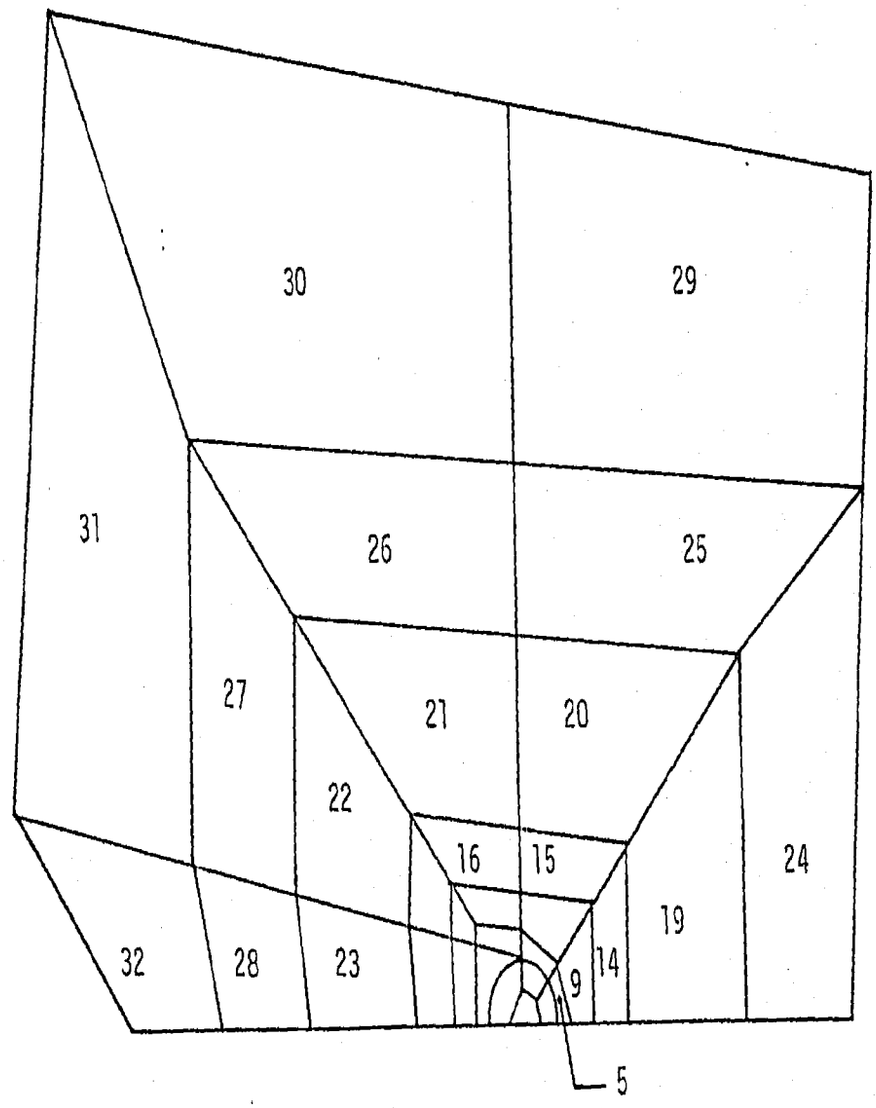

FIGURE 21 - ELEMENT NUMBERING OF FINITE ELEMENT GRID PATTERN
FOR x = 27.94 cm

CONTOUR VALUES (MJ/m^3)

1 - 6.76×10^1

2 - 8.96×10^1

3 - 1.03×10^2

4 - 1.24×10^2

5 - 1.45×10^2

6 - 1.59×10^2

7 - 1.86×10^2

8 - 2.00×10^2

9 - 2.07×10^2

10 - 2.14×10^2

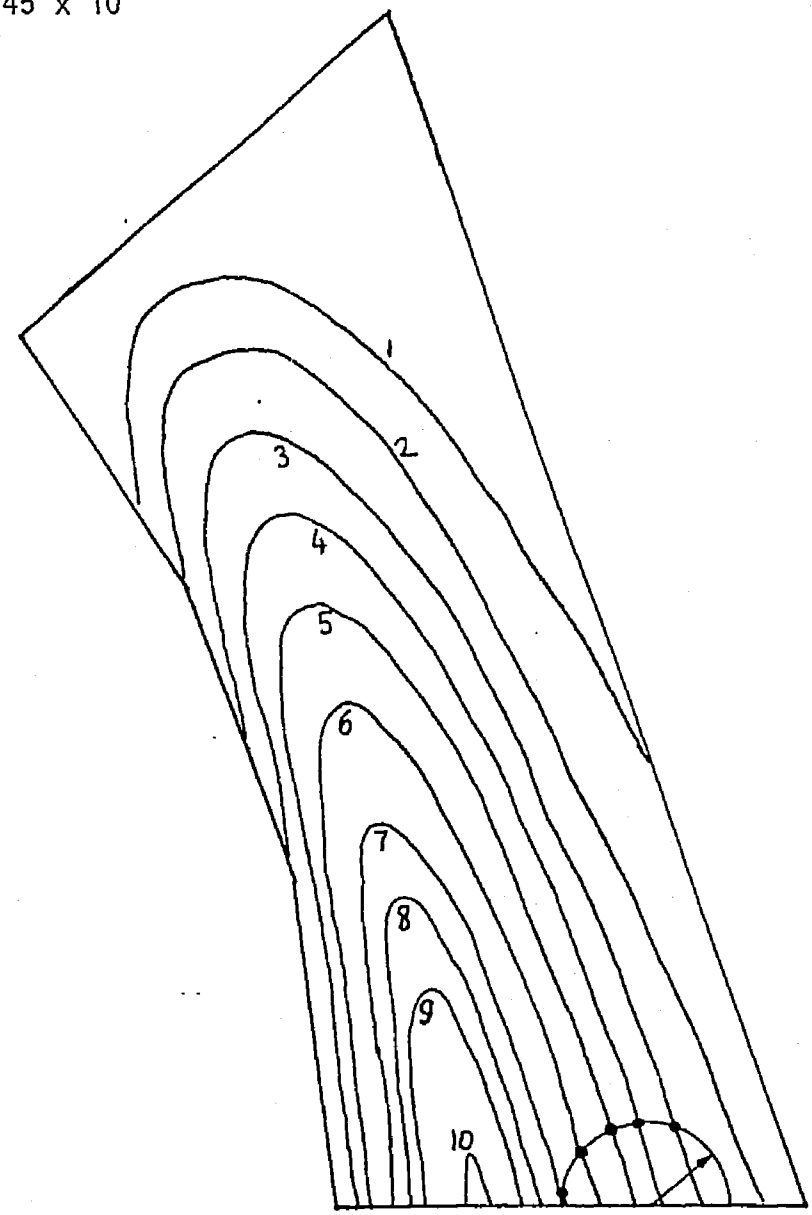

FIGURE 22(a) - STRAIN ENERGY DENSITY CONTOURS IN ELEMENT NUMBER 5 WITH RADIUS VECTOR LOCI INTERSECTING CONTOURS FOR r = 3.2 mm

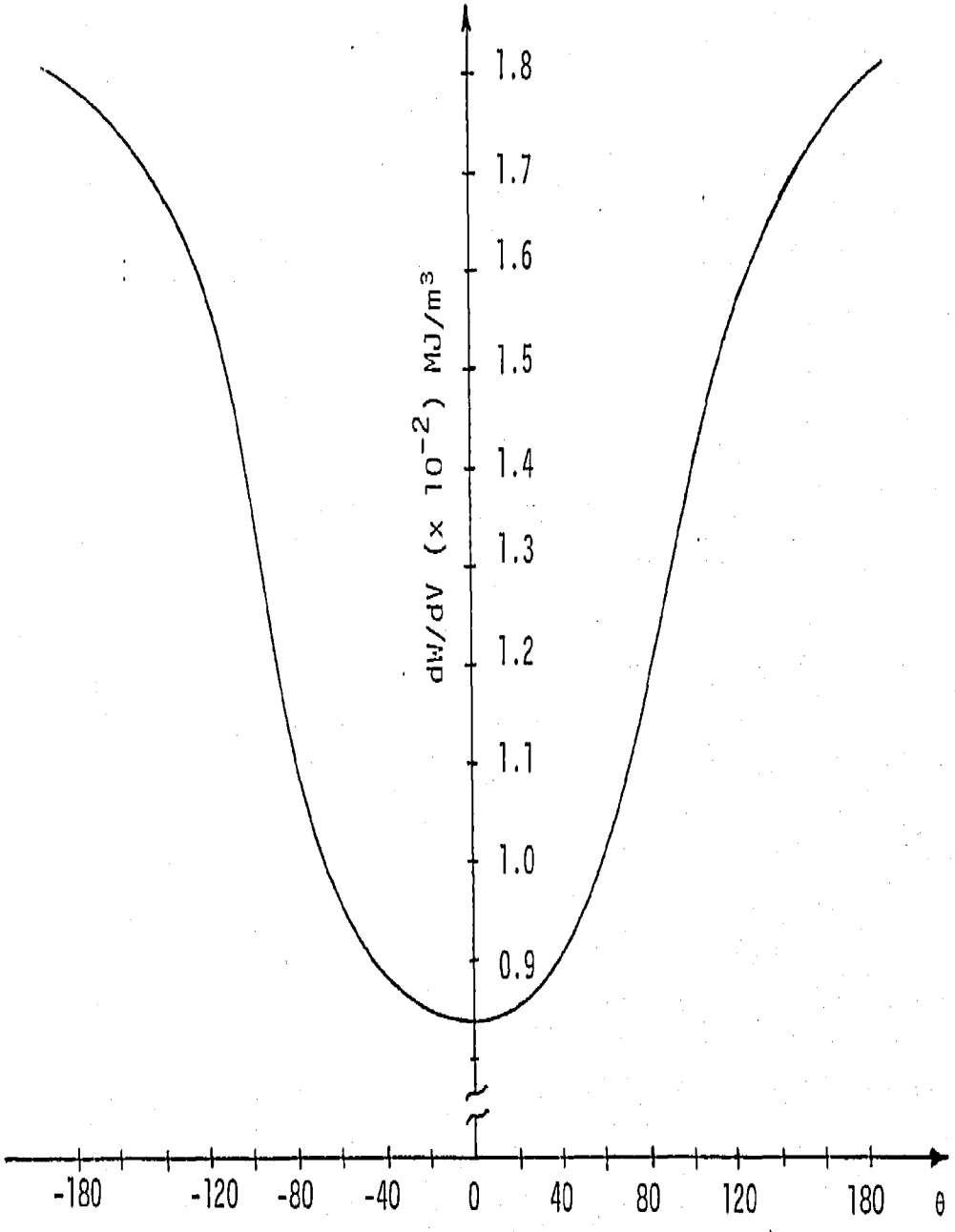

FIGURE 22(b) - VARIATION OF dW/dV FOR CONSTANT MAGNITUDE RADIUS VECTOR (r = 3.2 mm) AS A FUNCTION OF POLAR ANGLE θ

CONTOUR VALUES (MJ/m^3)

1 - 2.48×10^1

2 - 3.24×10^1

3 - 4.00×10^1

4 - 4.83×10^1

5 - 5.58×10^1

6 - 6.34×10^1

7 - 6.89×10^1

8 - 7.58×10^1

9 - 7.58×10^1

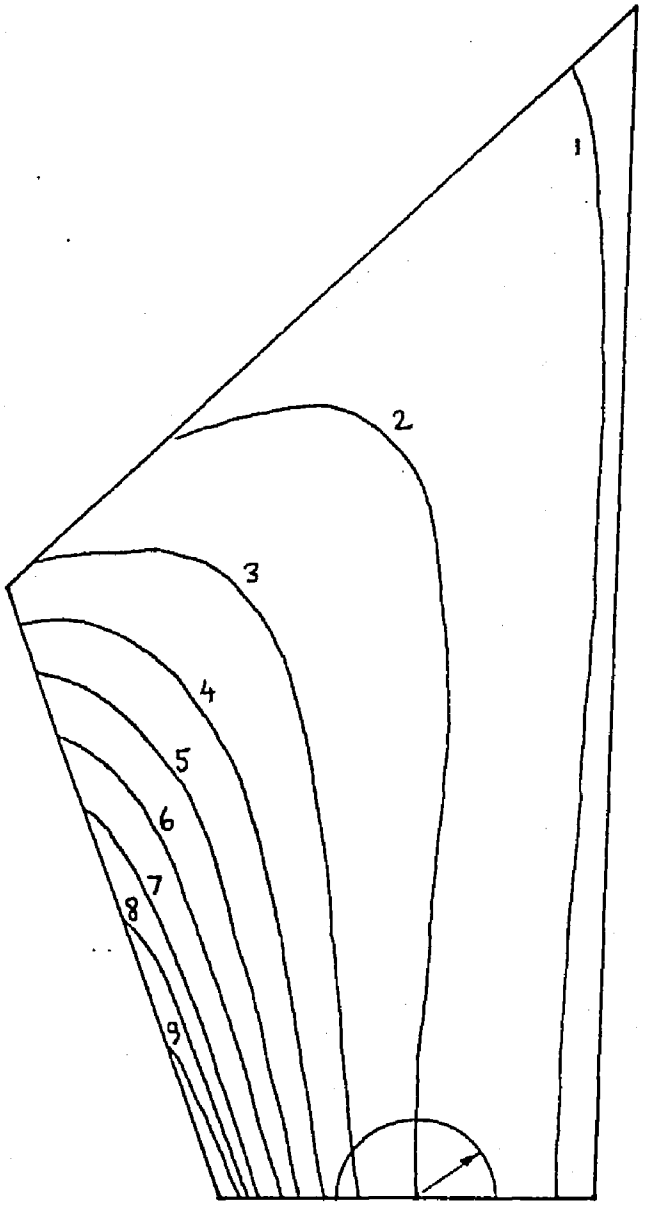

FIGURE 23(a) - STRAIN ENERGY DENSITY CONTOURS IN ELEMENT NUMBER 9 WITH RADIUS VECTOR LOCI INTERSECTING CONTOURS FOR r = 5.4 mm

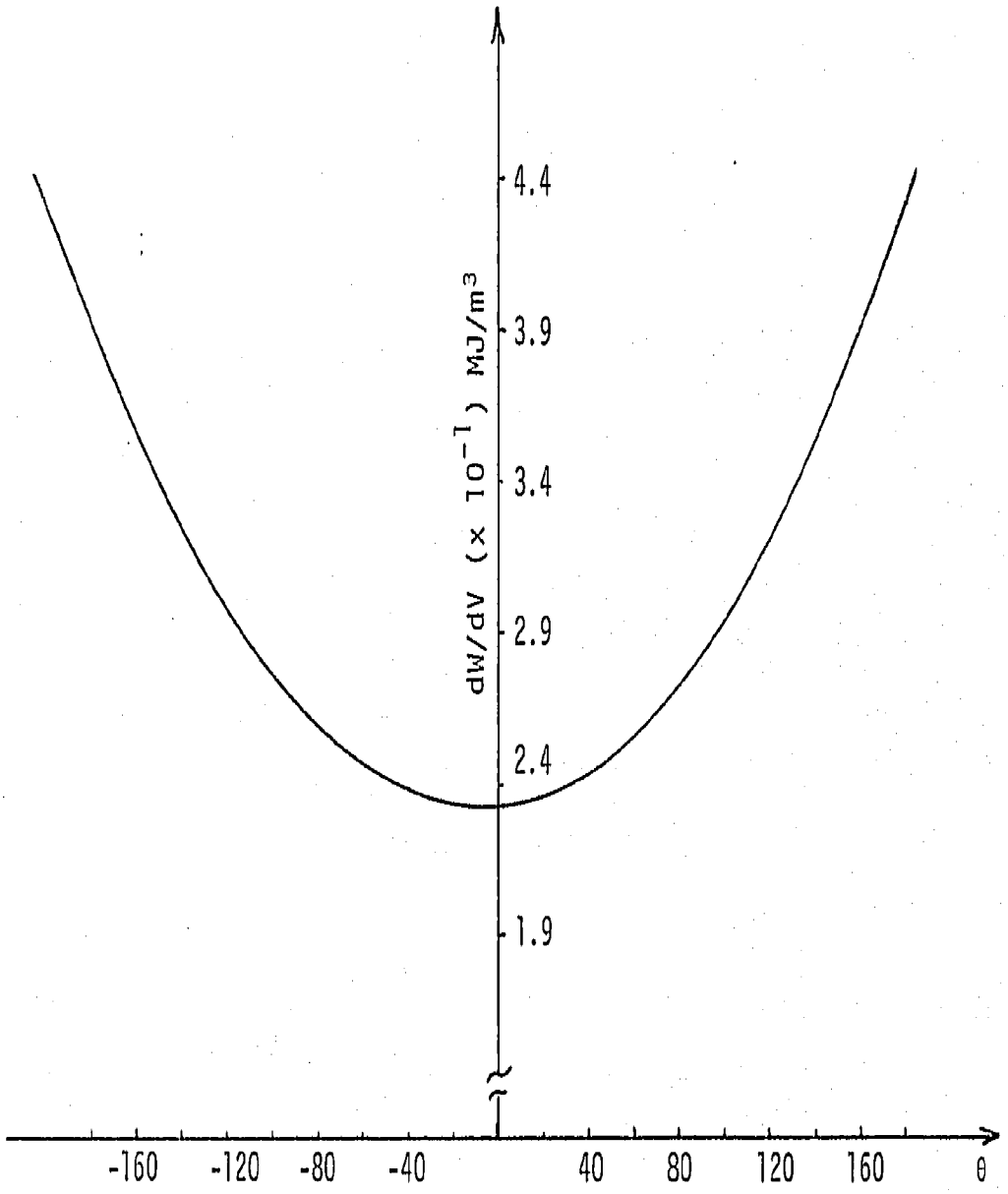

FIGURE 23(b) - VARIATION OF dW/dV FOR CONSTANT MAGNITUDE RADIUS VECTOR (r = 5.4 mm) AS A FUNCTION OF POLAR ANGLE θ

CONTOUR VALUES (MJ/m^3)

1 - 6.00

2 - 7.58

3 - 9.65

4 - 1.17×10^1

5 - 1.38×10^1

6 - 1.52×10^1

7 - 1.72×10^1

8 - 1.93×10^1

9 - 2.07×10^1

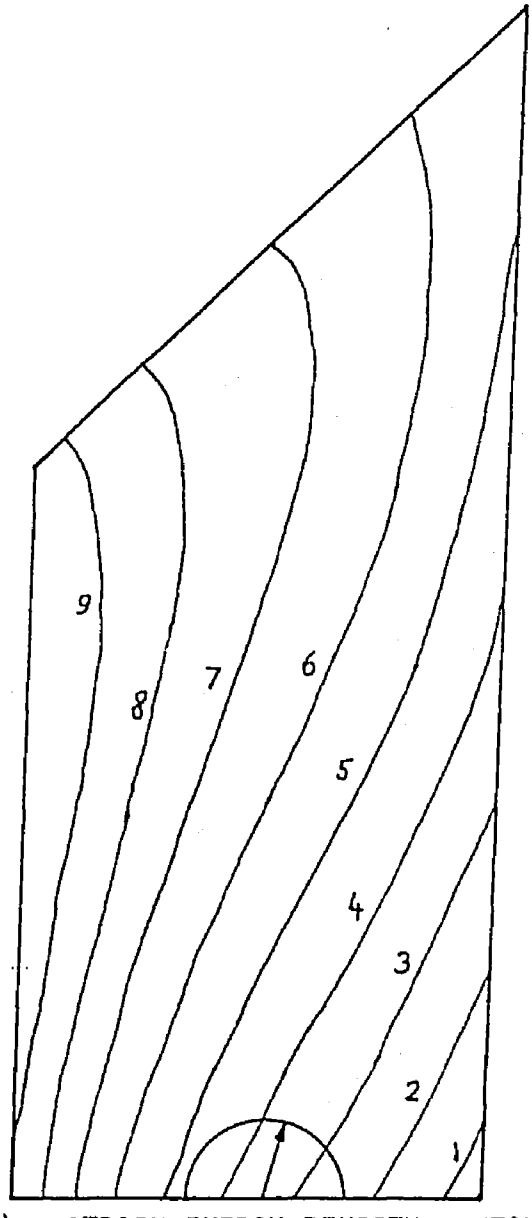

FIGURE 24(a) - STRAIN ENERGY DENSITY CONTOURS IN ELEMENT NUMBER 14 WITH RADIUS VECTOR LOCI INTERSECTING CONTOURS FOR r = 8.6 mm

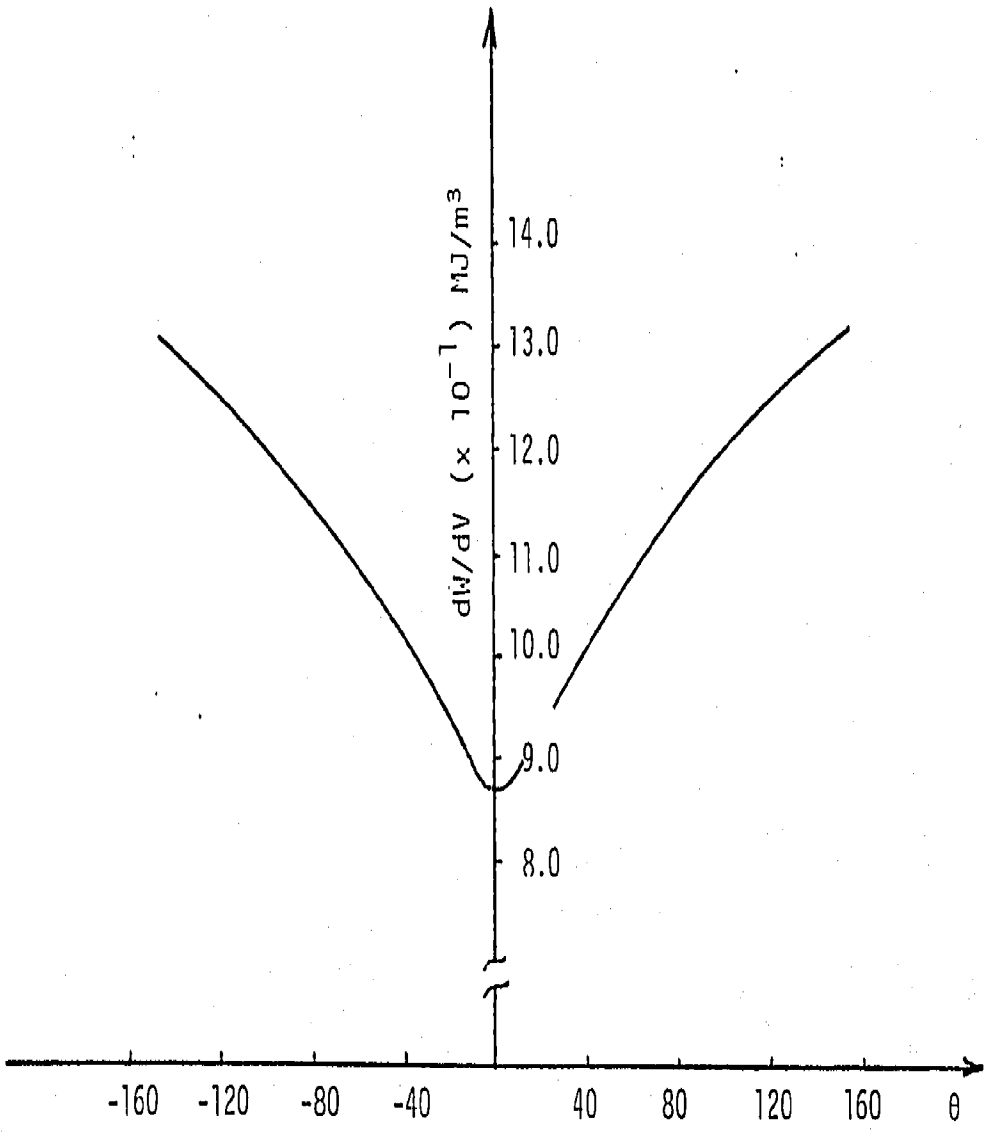

FIGURE 24(b) - VARIATION OF dW/dV FOR CONSTANT MAGNITUDE RADIUS VECTOR (r = 8.6 mm) AS A FUNCTION OF POLAR ANGLE θ

CONTOUR VALUES (MJ/m^3)

1 - 1.65

2 - 3.03

3 - 4.34

4 - 5.72

5 - 8.27

6 - 1.10×10^7

7 - 1.38×10^7

8 - 1.65×10^7

9 - 2.07×10^7

10 - 2.21×10^7

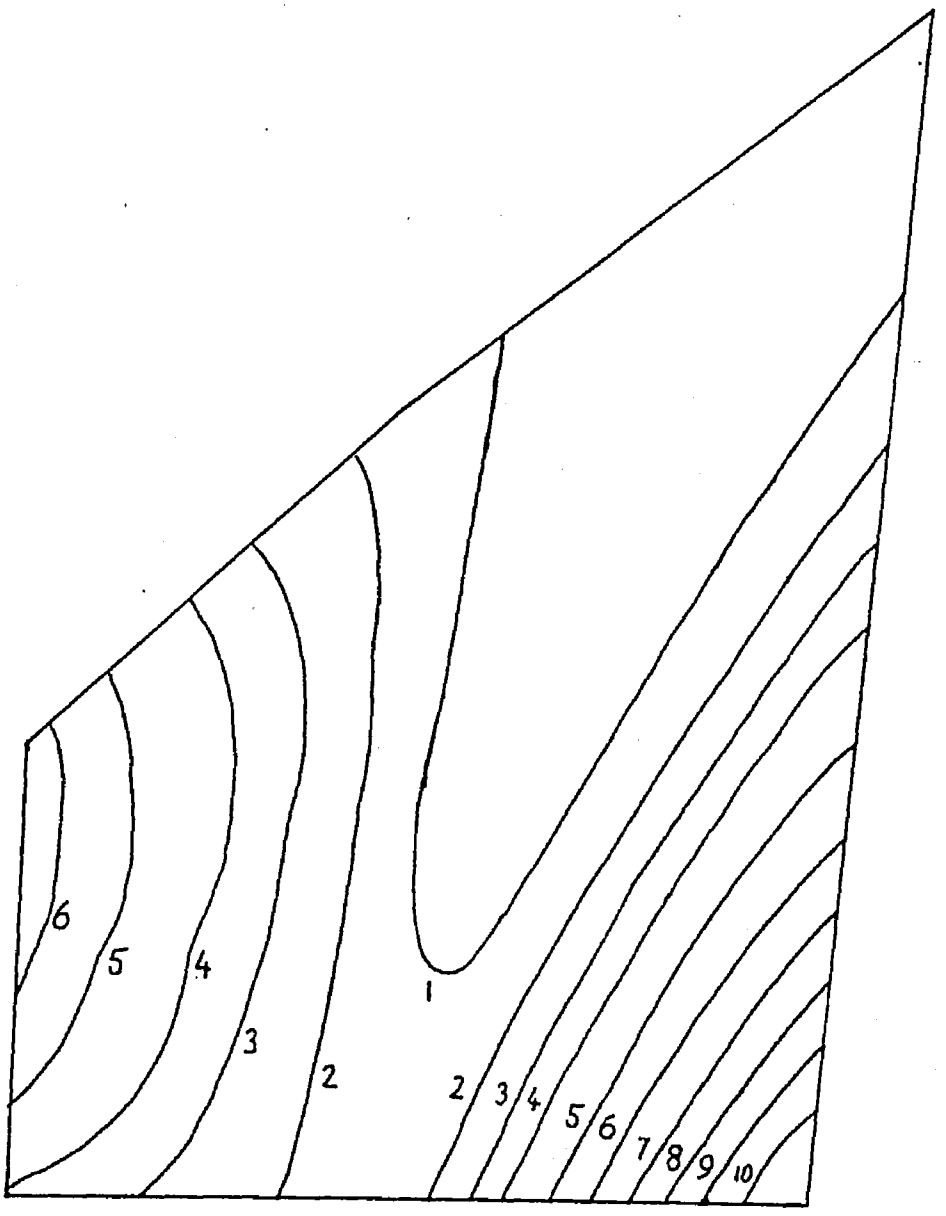

FIGURE 25 - STRAIN ENERGY DENSITY CONTOURS IN ELEMENTS 19 AND 24

CHAPTER VII - CONCLUSIONS AND FUTURE WORK

Thermoplastic stress analysis is performed on the problem of a moving energy source traversing across a prestretched plate. This is accomplished by means of the finite element technique such that the event is discretized to a finite number of time increments. The laser is modeled with a finite beam diameter. Material at the trailing path behind the laser is assumed to be permanently damaged such that its modulus of elasticity ($E_{effective}$) is reduced dramatically. This effect is analyzed in conjunction with the strain energy density failure criterion for each time increment in order to determine the critical combination of material, geometry and loading parameters that corresponds to global instability of the plate. A specific example is provided for a 7075-T651 aluminum plate under tension. Indeed, unstable fracture is predicted when the laser is about two thirds way across the plate. The prediction is based on the critical value of $(dW/dV)^*_c$ that accounts for the loss of energy due to plastic deformation.

Since the material in the damaged zone undergoes high strain rate, more data is required for future failure prediction that does not involve some of the assumptions made in this work. The translation of uniaxial tensile data to the nonhomogeneous local stress and strain field requires the general concept of the rate of change of volume element with respect to its surface area, i.e., dV/dA which can be written as

$$\frac{dV}{dA} = \frac{h_p\left(\frac{dW}{dV}\right)_p}{\frac{dW}{dV}} \tag{26}$$

in which dW/dV is calculated from equation (1) and h_p is a characteristic length corresponding to a homogeneous state of energy. The quantity $(dW/dV)_p$ is that given in equation (7). Equation (26) is a consequence of the strain energy density criterion that accounts for yielding and fracture simultaneously. It replaces the von Mises yield condition in the classical theory of plasticity. Such an extension, however, is beyond the scope of this work and will be left for future research.

REFERENCES

[1] Battista, A. D. and Shiner, W. H., "Production Laser Hole Drilling-Now", Thermal Machining Processes, Society of Manufacturing Engineers (1979), pp. 149-189.

[2] Enquist, R. D., "Effects of Lasers on Fracture of Materials", Fracture, edited by H. Liebowitz, Vol. 6 (1969), pp. 399-424.

[3] Matczyński, M. and Sih, G. C., "Prediction of Damage Sites Ahead of a Moving Heat Source", Defects, Fracture and Fatigue, edited by G. C. Sih and J. W. Provan, Martinus Nijhoff Publishers (1983), pp. 211-222.

[4] Carslaw, H. S. and Jaeger, J. C., Conduction of Heat in Solids, Oxford at the Clarendon Press, 1962.

[5] Sih, G. C., "A Special Theory of Crack Propagation: Methods of Analysis and Solution of Crack Problems", Mechanics of Fracture I, edited by G. C. Sih (1973), pp. XXI-XLV.

[6] Sih, G. C., "Analytical Modeling: Crack Growth Characteristics", Fracture Mechanics, edited by N. Perrone, H. Liebowitz, D. Mulville and W. Pilkey, University Press of Virginia, Charlottesville, 1978.

[7] Sih, G. C., "Strain Energy Density Factor Applied to Mixed Mode Crack Problems", International Journal of Fracture (1974), pp. 305-321.

[8] Sih, G. C., "Energy Density Concept in Fracture Mechanics", Engineering Fracture Mechanics, Vol. 5 (1973), pp. 1037-1040.

[9] Sih, G. C. and Macdonald, B., "Fracture Mechanics Applied to Engineering Problems - Strain Energy Density Fracture Mechanics, Vol. 6 (1974), pp. 361-386.

[10] Sih, G. C., Handbook of Stress Intensity Factors, Lehigh University, 1973.

[11] Kipp, M. E. and Sih, G. C., "The Strain Energy Density Failure Criterion Applied to Notched Elastic Solids", International Journal of Solids and Structures, Vol. 11 (1975), pp. 153-173.

[12] Theocaris, P. S., "Experimental Determination of the Core Region in Mixed Mode Fracture", Proceedings of the First USA-Greece Symposium on Mixed Mode Crack Propagation, edited by G. C. Sih and P. S. Theocaris, Sijthoff and Noordhoff (1981), pp. 21-36.

[13] Gifford, N. L. and Hilton, P. D., "Preliminary Documentation of PAPST-Nonlinear Fracture and Stress Analysis by Finite Elements", NSRDC-Preliminary Documentation, 1981.

[14] Sih, G. C. and Madenci, E., "Fracture Initiation Under Gross Yielding: Strain Energy Density Criterion", Engineering Fracture Mechanics, Vol. 18 (1983), pp. 667-677.

[15] Madenci, E., "Fracture Initiation in Weldments With or Without Crack-Like Imperfections", Unpublished M.S. Thesis, Lehigh University, 1982.

APPENDIX A - TEMPERATURE DISTRIBUTION FOR A LASER SPOT

The temperature distribution for a moving point heat source is

$$T(\xi_1,\xi_2) = \frac{Q_o}{2\pi\kappa h} e^{-\sigma\xi_1} K_o(\sigma r) \tag{A.1}$$

The temperature distribution for a circular laser spot is given by

$$T(\xi_1,\xi_2) = \int_A\int T(\overset{*}{\xi}_i)dA = \frac{Q_o}{2\pi\kappa h}\int_A\int e^{-\sigma\overset{*}{\xi}_1} K_o(\sigma\overset{*}{r})d\lambda d\eta \tag{A.2}$$

which was derived by making use of equation (A.1) as a Green's function with A being the cross section area of the laser spot. In equation (A.2), the quantities $\overset{*}{\xi}_1$ and $\overset{*}{r}$ stand for

$$\begin{aligned}\overset{*}{\xi}_1 &= \xi_1 - \lambda \\ \overset{*}{r} &= \sqrt{(\xi_1-\lambda)^2 + (\xi_2-\eta)^2}\end{aligned} \tag{A.3}$$

APPENDIX B - STRAIN ENERGY DENSITY TABLES

In what follows, the strain energy density functions dW/dV ahead of the laser with its center located at x = 7.62, 15.24 and 22.86 cm are given.

In Tables 4 and 5, the strain energy density functions decrease monotonically with the distance away from the laser.

TABLE 4 - STRAIN ENERGY DENSITY VALUES AHEAD OF THE LASER BEAM FOR x = 7.62 cm

Distance from the Center of the Laser Beam (cm)	Distance from the Left Reference Point (cm)	dW/dV (MJ/m^3)
2.54	10.16	7.52
3.81	11.43	1.53
5.08	12.70	8.18×10^{-1}
7.62	15.24	4.51×10^{-1}
15.24	22.86	2.82×10^{-1}
27.94	35.56	2.08×10^{-1}
38.10	45.72	1.29×10^{-1}

A minimum in dW/dV is detected at 15.24 cm ahead of the laser when x = 22.86 cm, Table 6. However, fracture still does not occur because the corresponding value of $(dW/dV)^*_{min}$ is less than $(dW/dV)^*_c$.

TABLE 5 - STRAIN ENERGY DENSITY VALUES AHEAD OF THE LASER BEAM FOR x = 15.24 cm

Distance from the Center of the Laser Beam (cm)	Distance from the Left Reference Point (cm)	dW/dV (MJ/m^3)
2.54	17.78	1.55×10^{1}
3.81	19.05	4.79
5.08	20.32	2.44
8.89	24.13	7.41×10^{-1}
15.24	30.48	2.60×10^{-1}
21.59	36.83	1.30×10^{-1}
30.48	45.72	3.05×10^{-2}

TABLE 6 - STRAIN ENERGY DENSITY VALUES AHEAD OF THE LASER BEAM FOR x = 22.86 cm

Distance from the Center of the Laser Beam (cm)	Distance from the Left Reference Point (cm)	dW/dV (MJ/m^3)
2.54	25.40	2.96×10^{1}
3.81	26.67	9.02
5.08	27.94	5.62
10.16	33.02	1.16
15.24	38.10	1.75×10^{-1}
22.86	45.72	2.82

VITA

Metin Ozen was born on January 31, 1958 in Izmir, Turkey to Ahmet and Fitnat Ozen. He went to elementary and high school in Izmir and graduated from Izmir Anadolu Lycée in May 1976.

After attending courses in Istanbul Technical University, Turkey and Wilkes College, Pennsylvania, Mr. Ozen entered Lehigh University in January 1980. He received a Bachelor of Science in Mechanical Engineering in January 1982. As a graduate student, Mr. Ozen worked as a teaching assistant for Mathematics and Mechanical Engineering Departments and as a research assistant for the Institute of Fracture and Solid Mechanics at Lehigh University.